回音壁模式半导体微腔激光器

黄永箴

中国科学院半导体研究所
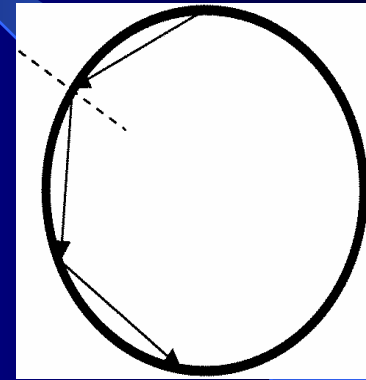
集成光电子学国家重点联合实验室

一、绪论

Theory of Sound

St. Paul's Cathedral

L. Rayleigh，The problem of the whispering gallery, *Phil. Mag.*, **20**, 1001(1910)
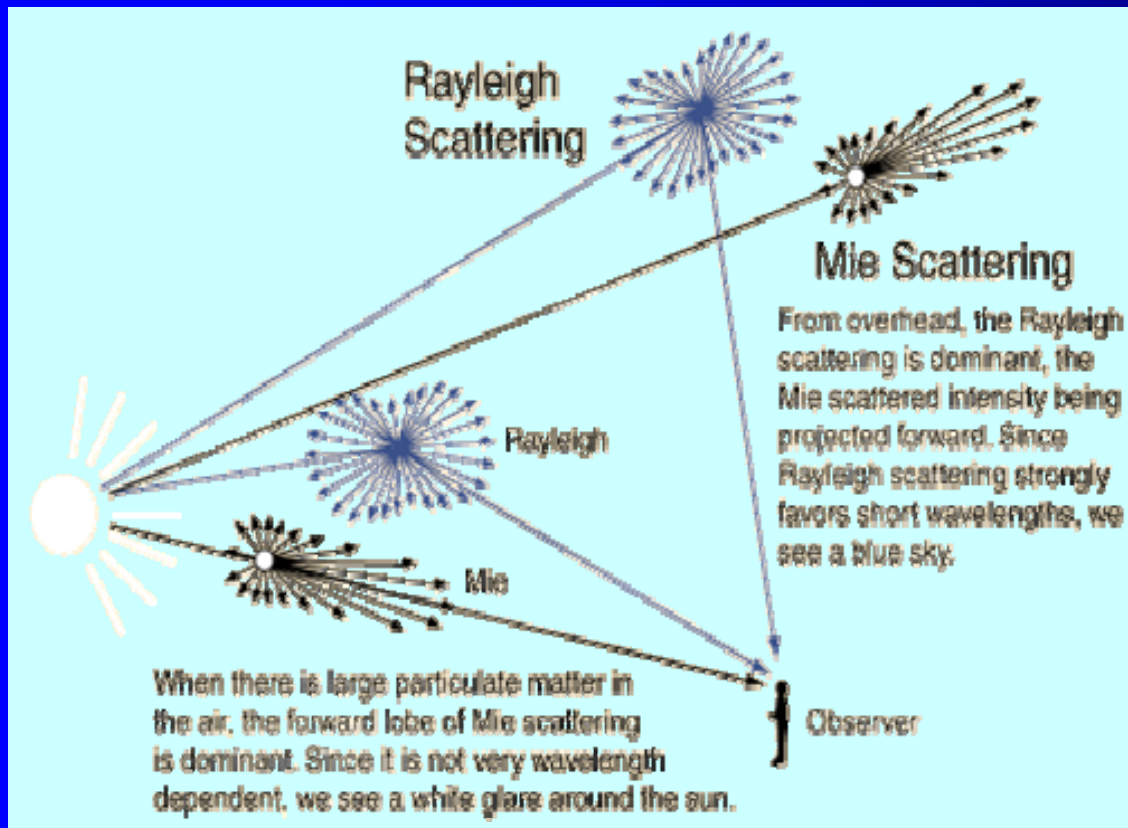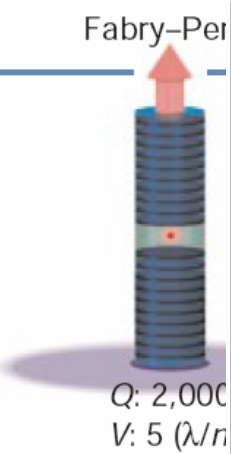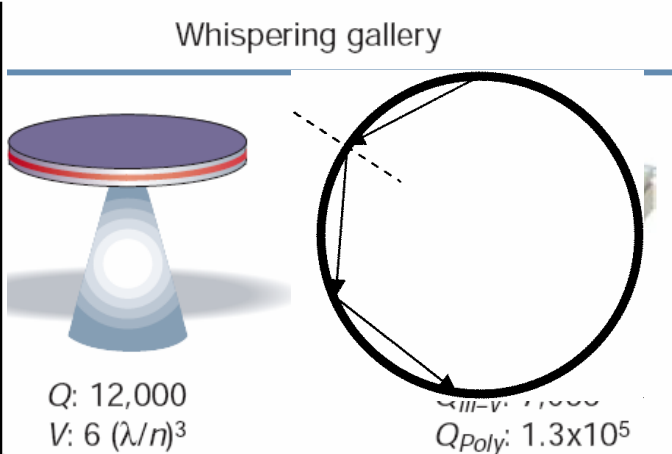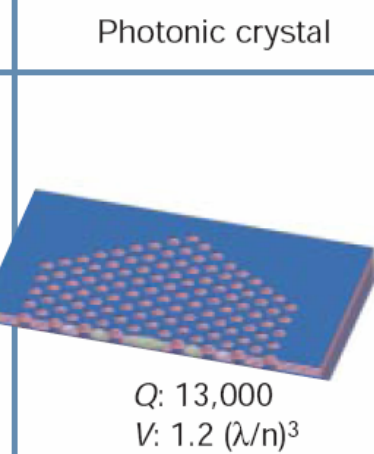
Mie Scattering:

Light scattering at particle with sizes larger than a wavelength, such as water drop in clouds, produces a pattern like an antenna lobe—

related to optical modes confined in a ball.

Rayleigh
Scattering

Mie Scattering

From overhead, the Rayleigh scattering is dominant, the Mie scattered intensity being projected forward. Since Rayleigh scattering strongly favors short wavelengths, we see a blue sky.

Rayleigh

Mie

When there is large particulate matter in the air, the forward lobe of Mie scattering is dominant. Since it is not very wavelength dependent, we see a white glare around the sun.

Observer

Mie G, Ann. Phys., 1908, 25(4):377

微腔的种类

- 法布里－珀罗(Fabry-Pérot, FP)腔：VCSEL
- 回音壁 (Whispering-Gallery, WG)模式腔:
  微盘、微环、微柱、微球、多边形腔

- 光子晶体(Photonic Crystal, PC)微腔

	Fabry–Per...	Whispering gallery	Photonic crystal
High Q	Q: 2,000 V: 5 (λ/n)³	Q: 12,000 V: 6 (λ/n)³ Q_III–V: ... Q_Poly: 1.3×10⁵	Q: 13,000 V: 1.2 (λ/n)³

K. J. Vahala, Nature vol.424, p. 839 (2003).

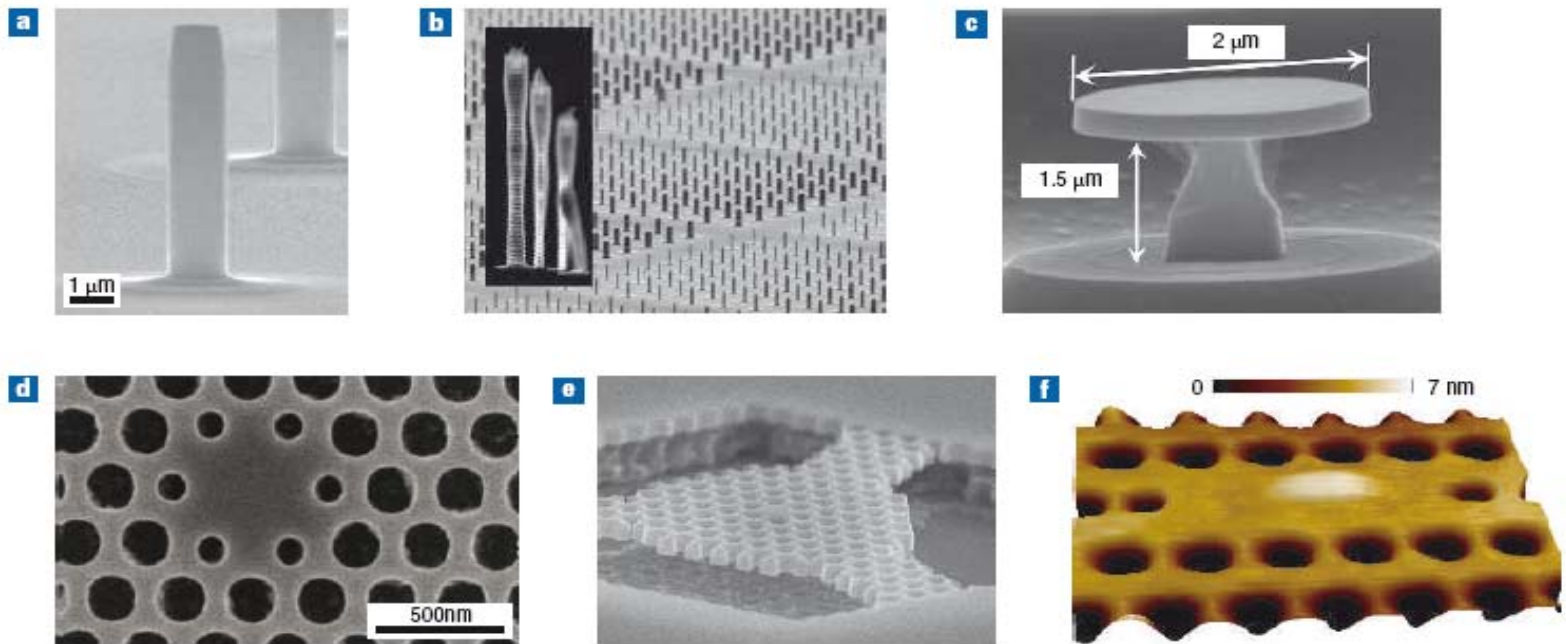注：品质因子Q，定义为一个谐振周期腔内存储能量的时间平均值和向外辐射的能量之比。Q越大，腔本征损耗越小

Figure 3 Scanning-electron-microscope images of semiconductor cavities. **a,b**, Pillar microcavities. **c**, microdisks. **d–f**, Photonic-bandgap defect cavities. The structures were fabricated at: **a**, University of Würzburg; **b,c,e**, CNRS-LPN (UPR-20); **d**, Univ. Cambridge; **f**, UCSB/ETHZ. (Image sources and permissions: **a**, Ref. 56. **c**, Ref. 51, copyright (2005) APS. **d**, Ref. 47, copyright (2006) AIP. **e,f**, Ref. 48)
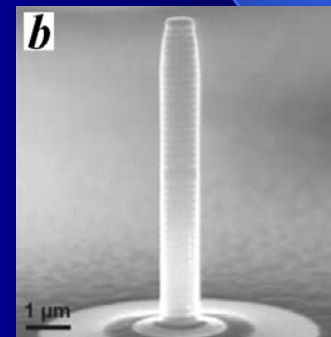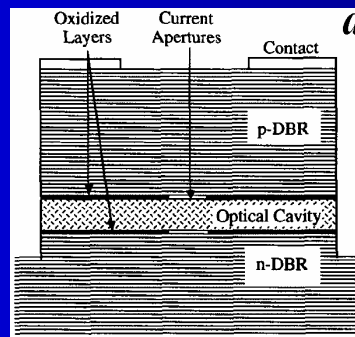
huang4

光学微腔器件的发展和研究现状

A. 光学微腔激光器

1. VCSEL

1979年InGaAsP材料77K下脉冲电注入激射；

1983年GaAs材料77K下脉冲电注入激射，同年室温脉冲激射；
1988年实现850nm的GaAs材料室温连续工作；

1998年，纳米尺度的VCSEL结构圆柱，研究自发辐射的增强或抑制，及单光子光源。

2. 微盘类激光器

1992年低温光泵浦下实现了激射。
1992年室温下实现了脉冲电注入激射
1993年室温脉冲光泵浦激射
1998年室温连续电注入激射，阈值电流150μA
2000年室温连续电注入激射，阈值电流40μA

研究背景和意义

1. 通信

现代光信息技术的飞速发展对高速率、低功耗、小型化的光子集成器件的研发提出了要求。

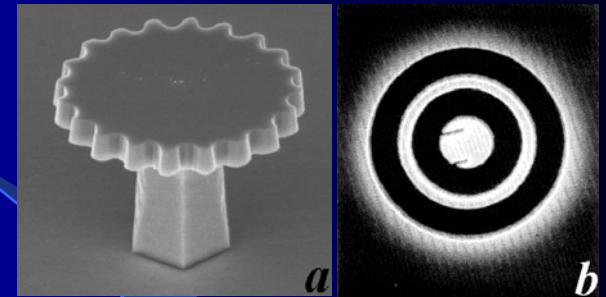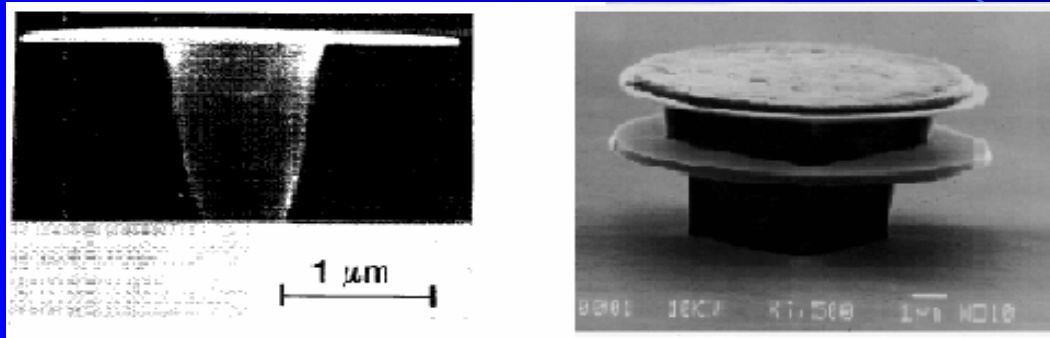各种功能器件得到广泛关注：激光源（微型、单模、低阈值），光学滤波器（微型、窄线宽、大自由谱域、可调谐）、光开关（微型、高速）、光调制器（微型、高速）等。
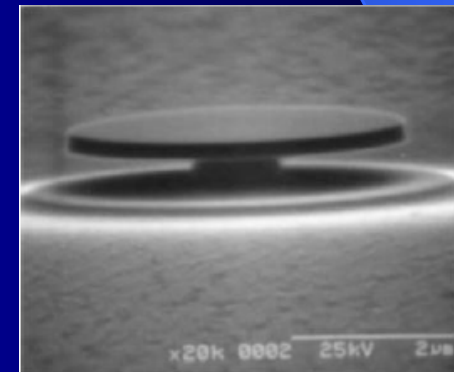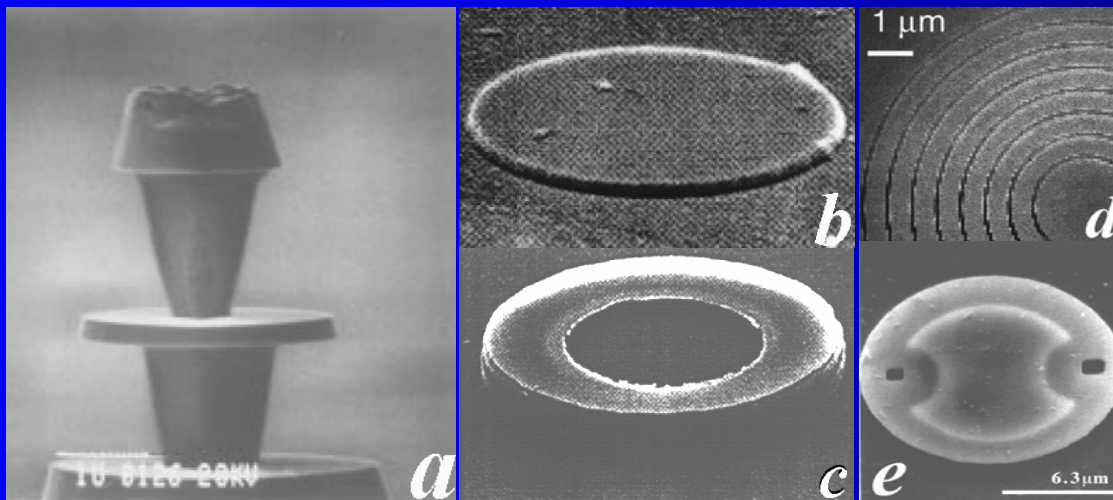
2. 传感

环境保护、安全系统等需要微型、可调谐和高灵敏度的传感器

3. 物理研究,单光子源,量子信息处理

研究腔量子电动力学和控制自发辐射需要超高品质因子的微型腔。

Whispering-Gallery Mode (WGM)

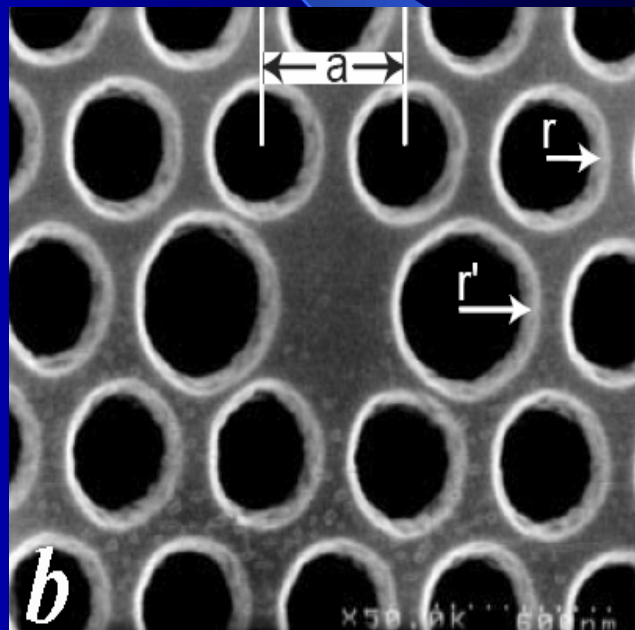S. L. McCall et al, Appl. Phys. Lett., vol.60, 289 (1992), Electron. Lett., vol.28, p.1010(1992)
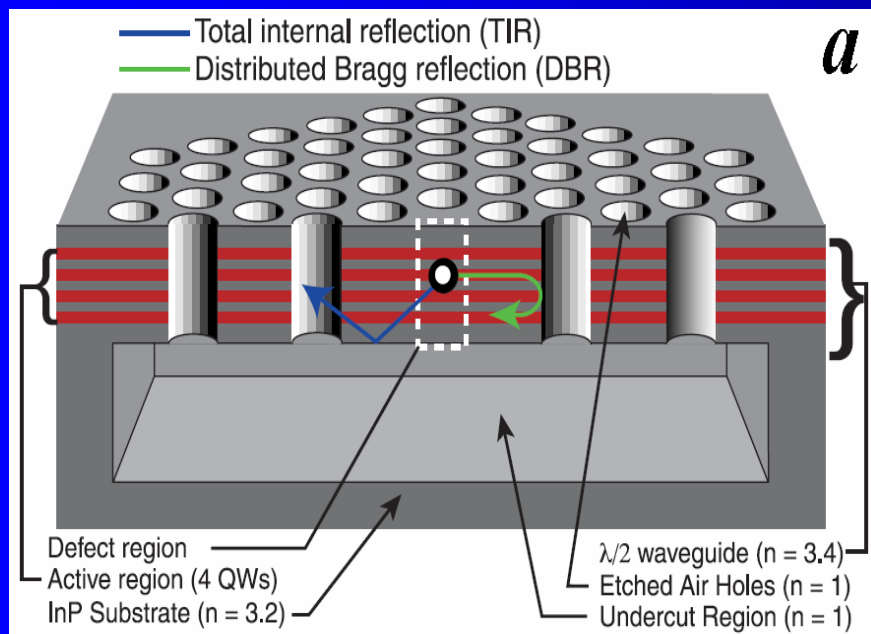
P. Michler et al, Science, vol. 290, p.2282(2000)

光子晶体微腔激光器

1999年低温脉冲光泵浦激射，阈值功率6.75mW
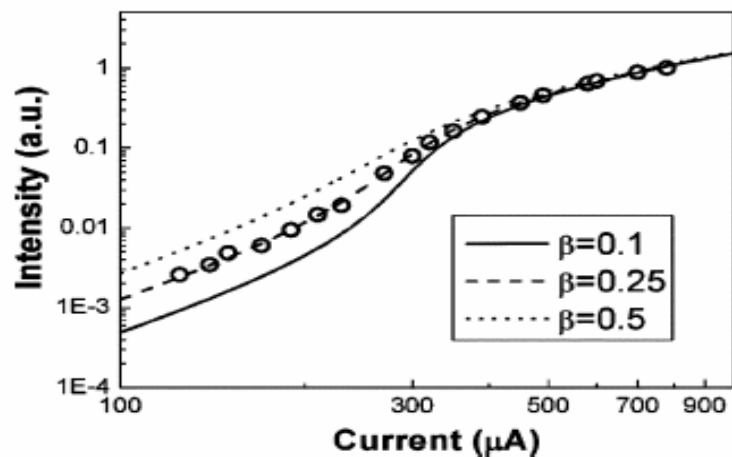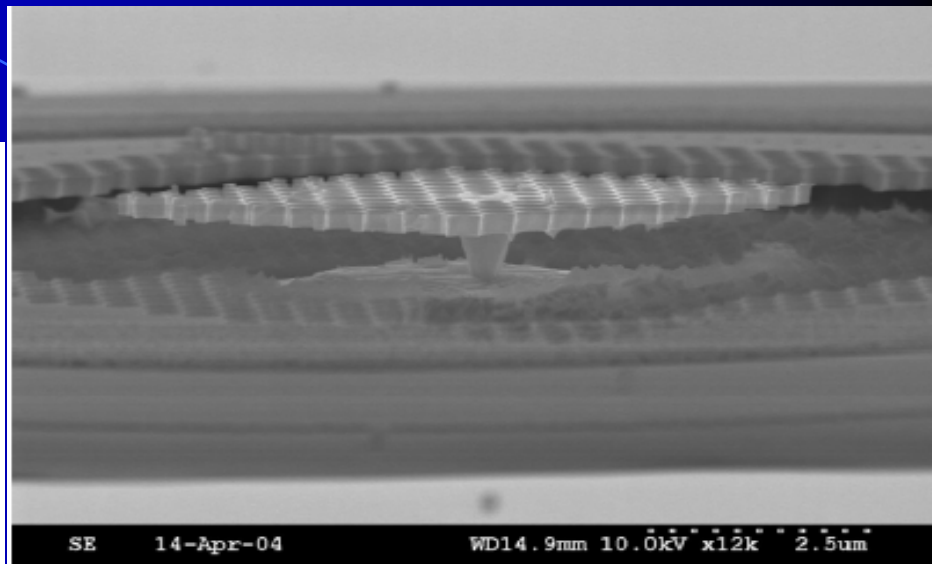2000年室温脉冲电注入激射，阈值电流300μA
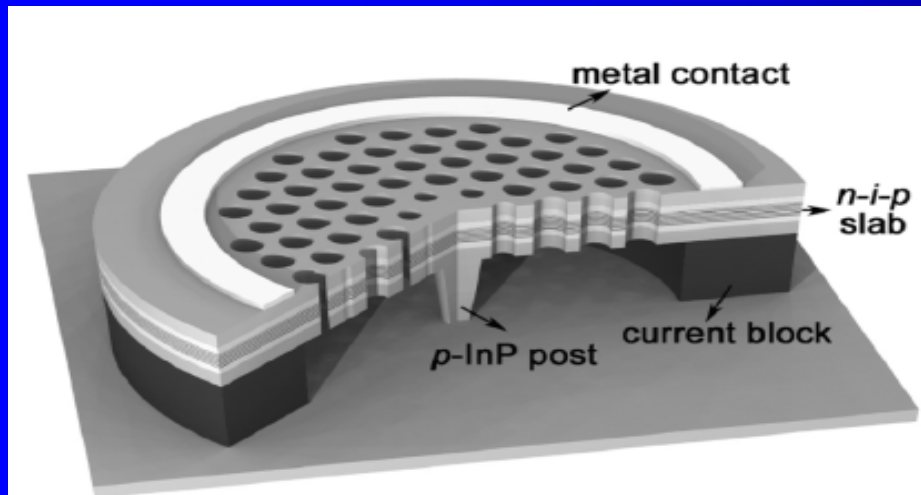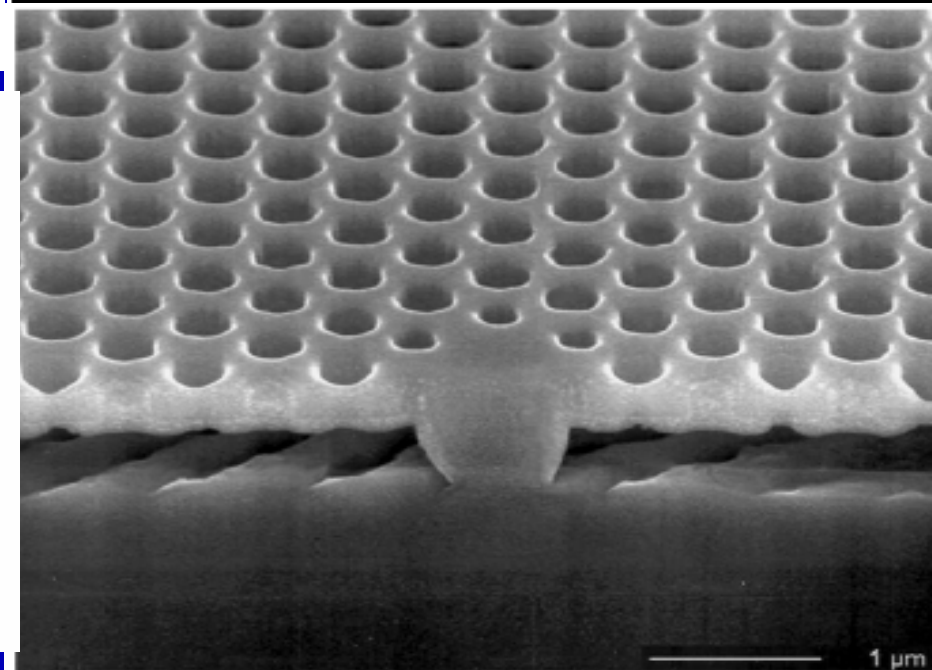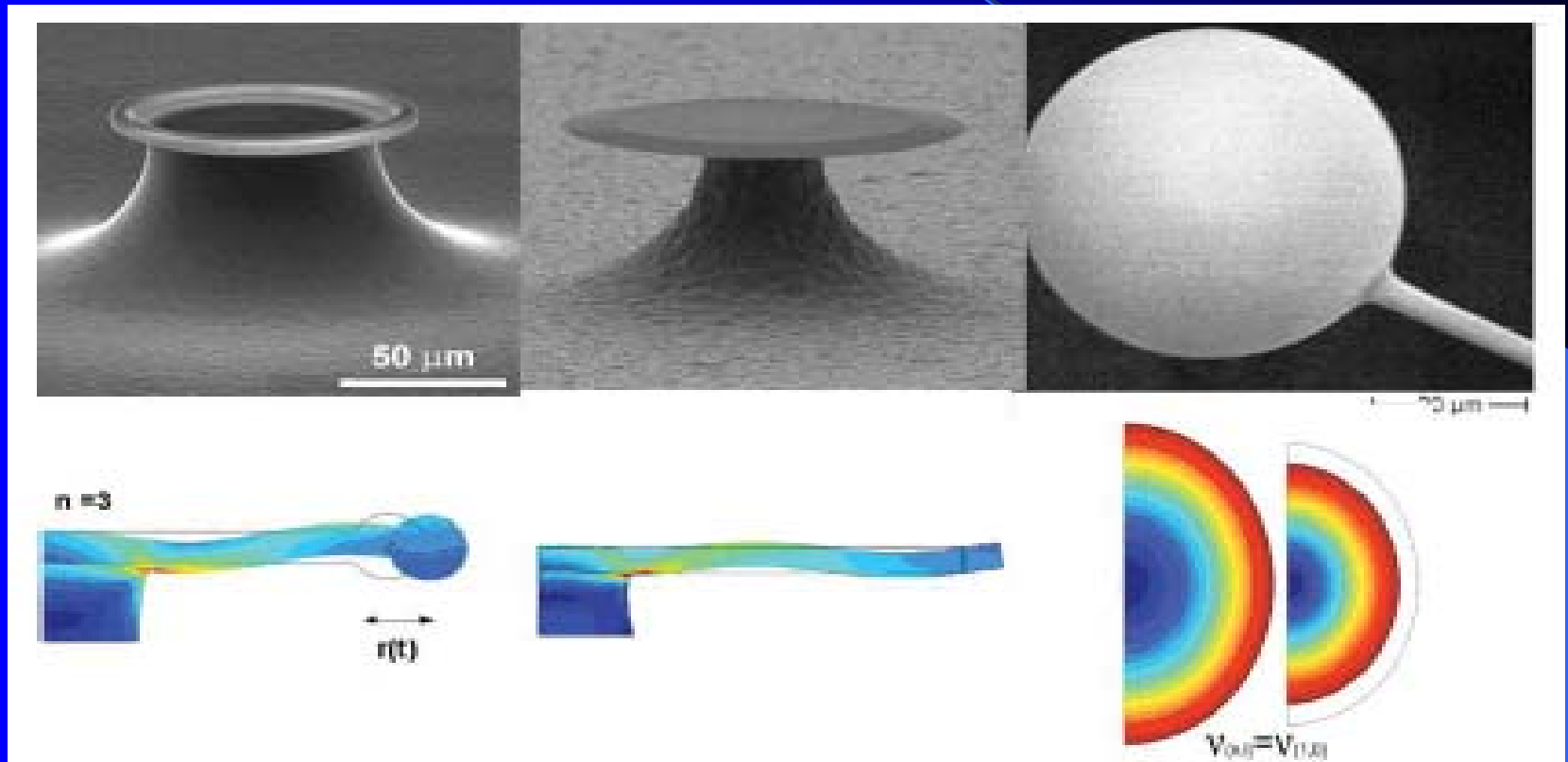2004年室温脉冲电注入激射，自发辐射因子0.25

电注入光子晶体微腔激光器

Fig. 14. Comparison of the measured $L-I$ curves (dots) with those obtained from the rate equations (lines) for the monopole mode.

The coupling of mechanical and optical degrees of freedom via radiation pressure has been a subject of early research in the context of gravitational wave detection.

T.J. Kippenberg and K.J. Vahala, "Cavity opto-mechanics" Optics Express, vol.15, p.17172(2007)
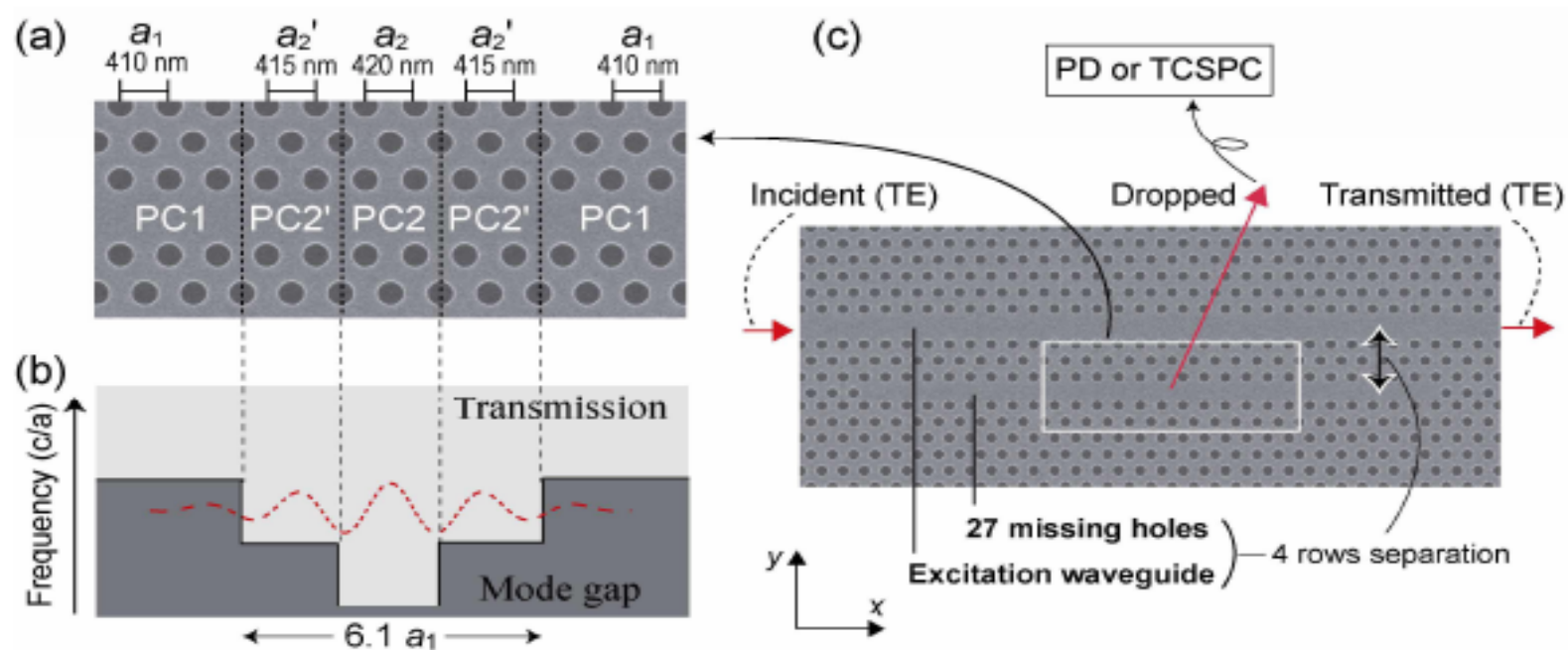
Fig. 1. (a). SEM image of the nanocavity with a two-step heterostructure. PC1 has a triangular-lattice structure with a lattice constant of a_1. PC2 and PC2' have a deformed triangular-lattice structure with lattice constants of a_2 and a_2' in the x-direction; they retain the same lattice constant as PC1 in the y-direction in order to satisfy lattice-matching conditions. (b) Schematic view of the band diagram along the x-direction for the line defect in Fig. 1(a). The ground-state nanocavity mode mainly exists in the waveguide section formed by PC2 and PC2'. (c) SEM image of the region around the nanocavity and schematic picture of the transmission spectroscopy experiment.

高**Q**值的光子晶体微腔

K. Hennessy, et al, "Quantum nature of a strongly coupled single quantum dot–cavity system," Nature, vol.445, p.896(2007)
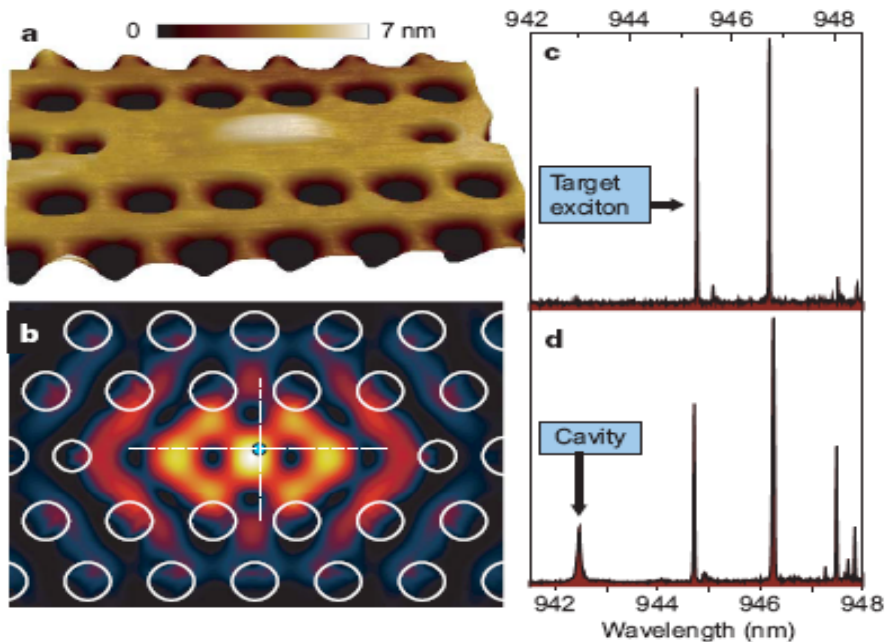

Figure 1 | Positioning a photonic crystal cavity mode relative to a single buried QD. a, AFM topography of a photonic crystal nanocavity aligned to a hill of material on the surface arising from a QD buried 63 nm below. The height scale is depicted by the colour bar. b, Electric field intensity of the photonic crystal cavity mode showing that the location of the buried QD, indicated by the teal dot, overlaps the field maximum. The field intensity ranges from zero (black) to a maximum (white), going through blue, red and yellow. c, Photoluminescence spectrum before cavity fabrication of a single QD, which was selected for cavity coupling on the basis of clear emission from a few discrete excitonic transitions. d, Photoluminescence spectrum from the same QD after cavity fabrication, showing emission from the cavity at 942.5 nm.
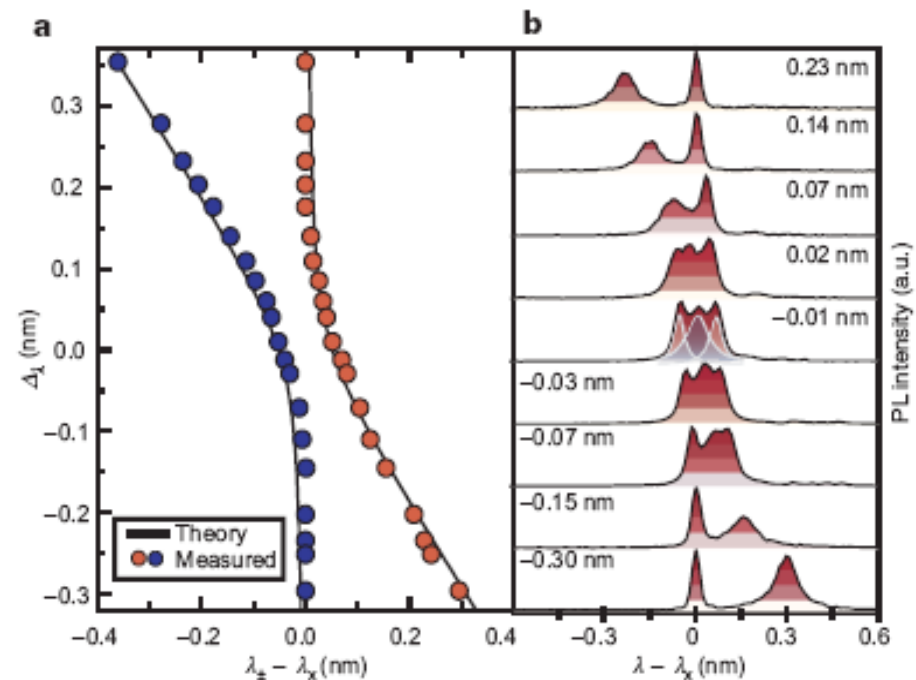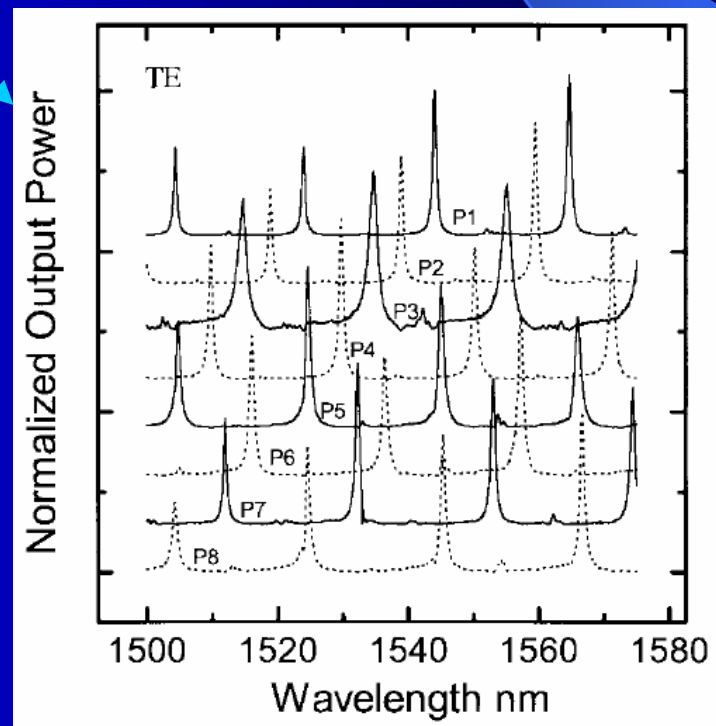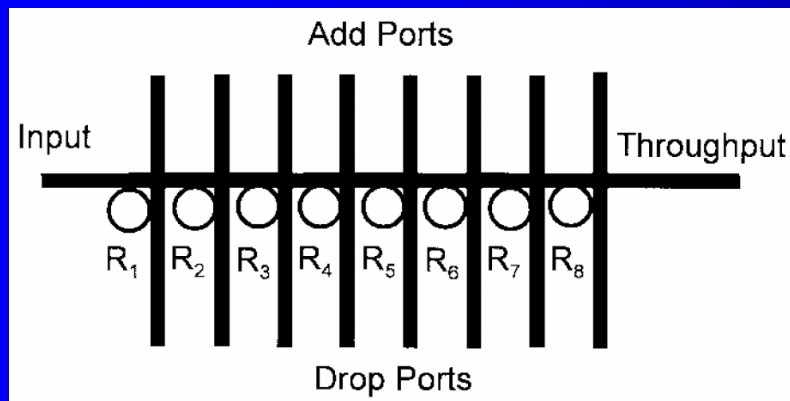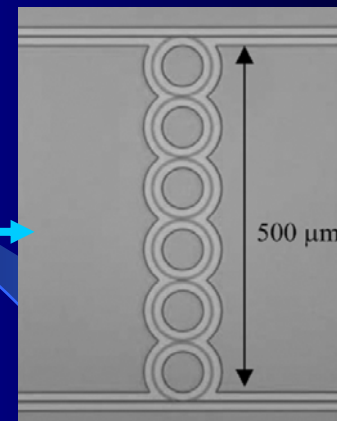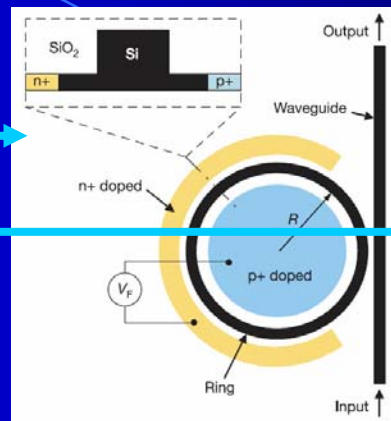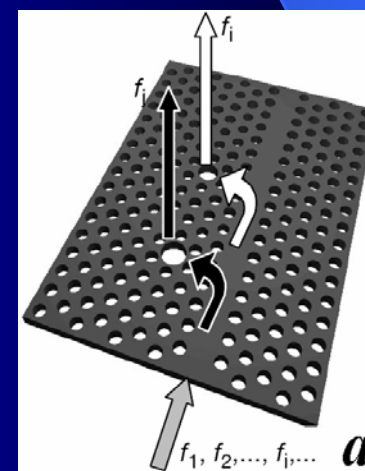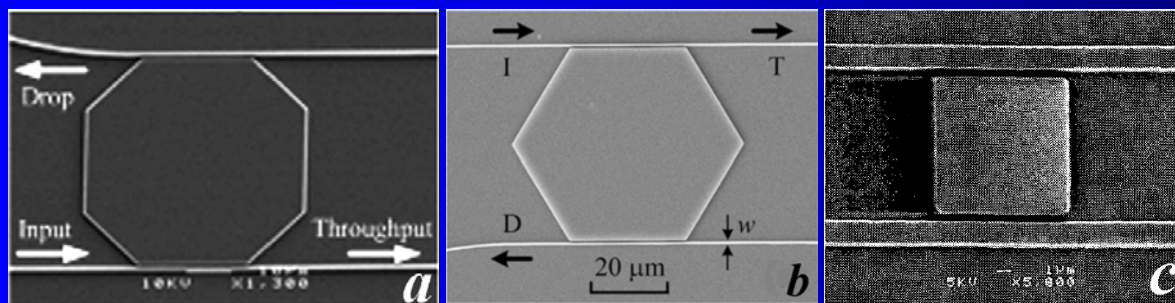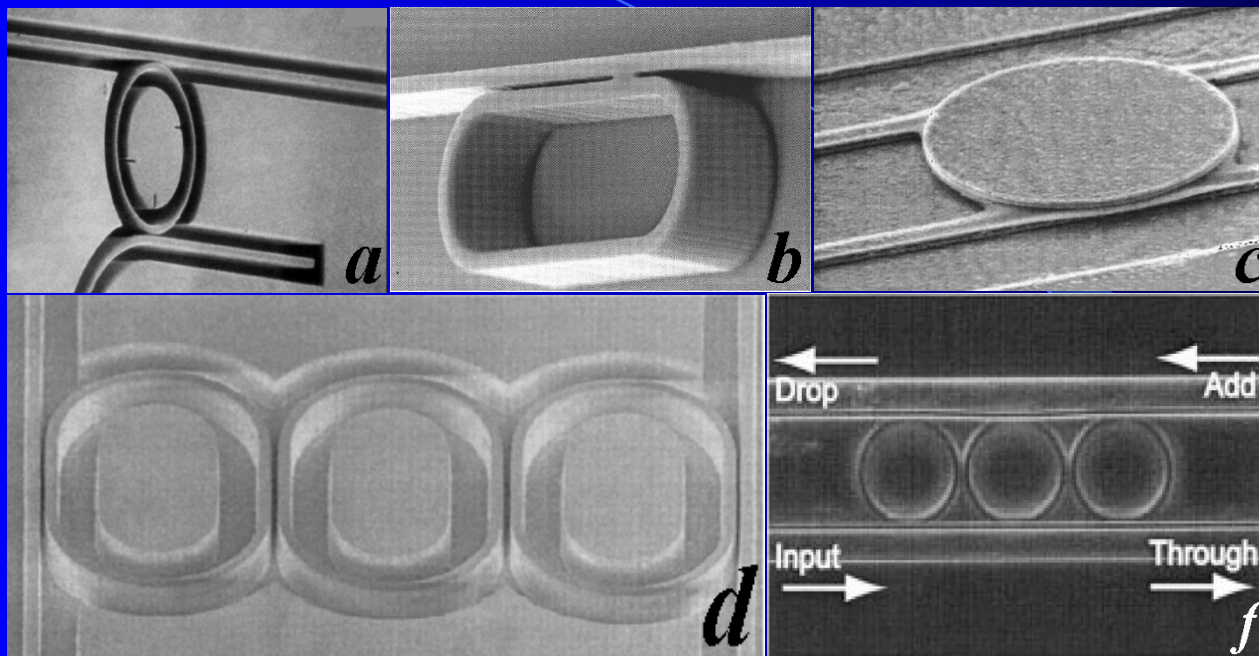
Figure 3 | Characteristics of the strong-coupling regime in the spectral domain. a, Wavelength of the polaritons for various detunings, Δ_λ. Calculated spectral peak positions describing the strongly coupled system are plotted as solid lines, with measured peak positions extracted from photoluminescence plotted in red and blue dots. b, Spectra of the two anticrossing polariton states near zero detuning. An additional peak is identified as the pure photonic state of the cavity. Values of Δ_λ are shown for each spectrum. PL, photoluminescence; a.u., arbitrary units.
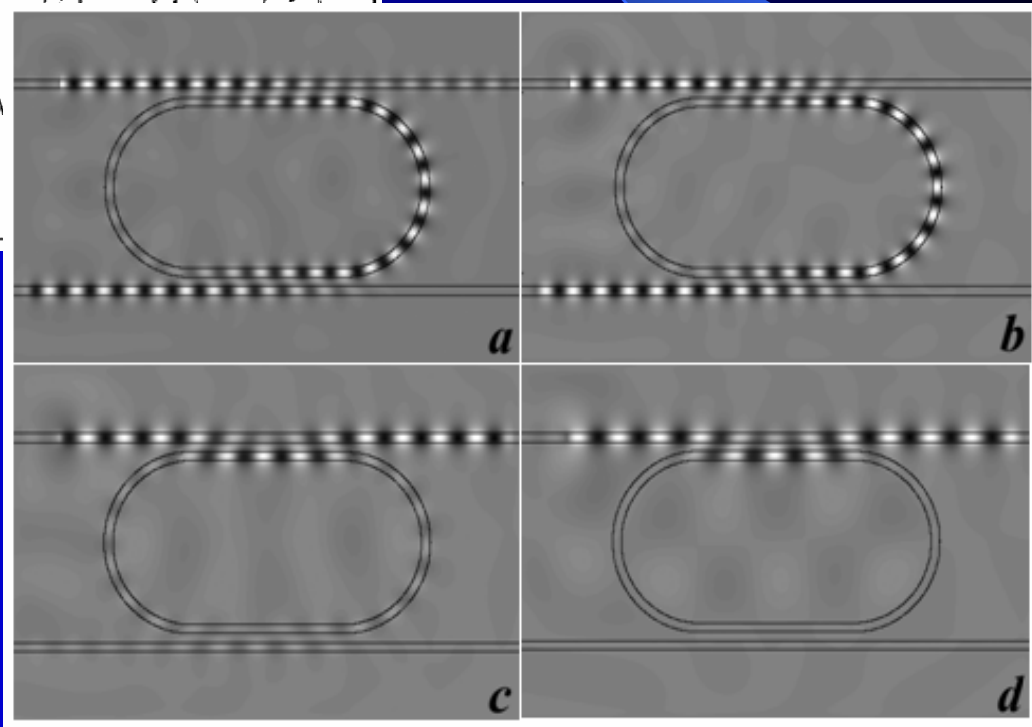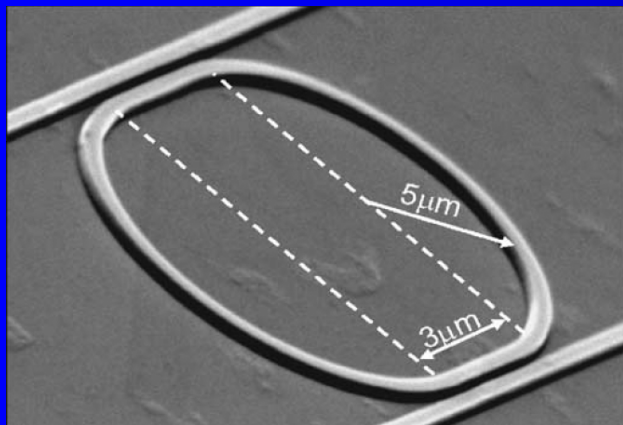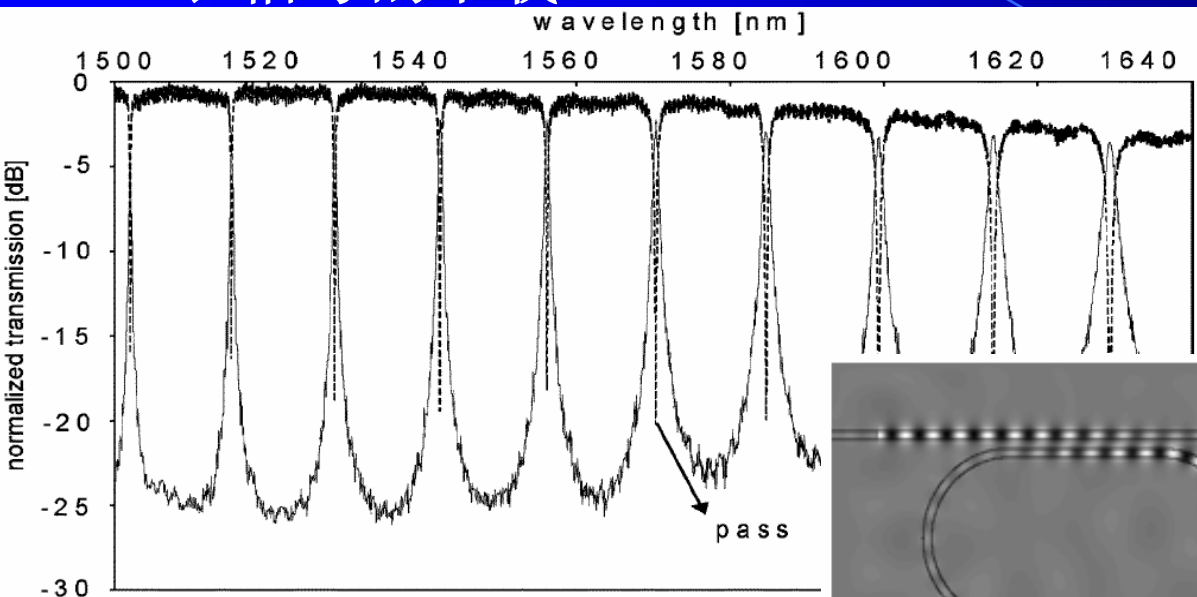
B. 光学微腔耦合器

- 滤波器
- 调制器
- 延迟器
- 逻辑门
- 光开关

各类典型微腔滤波器结构
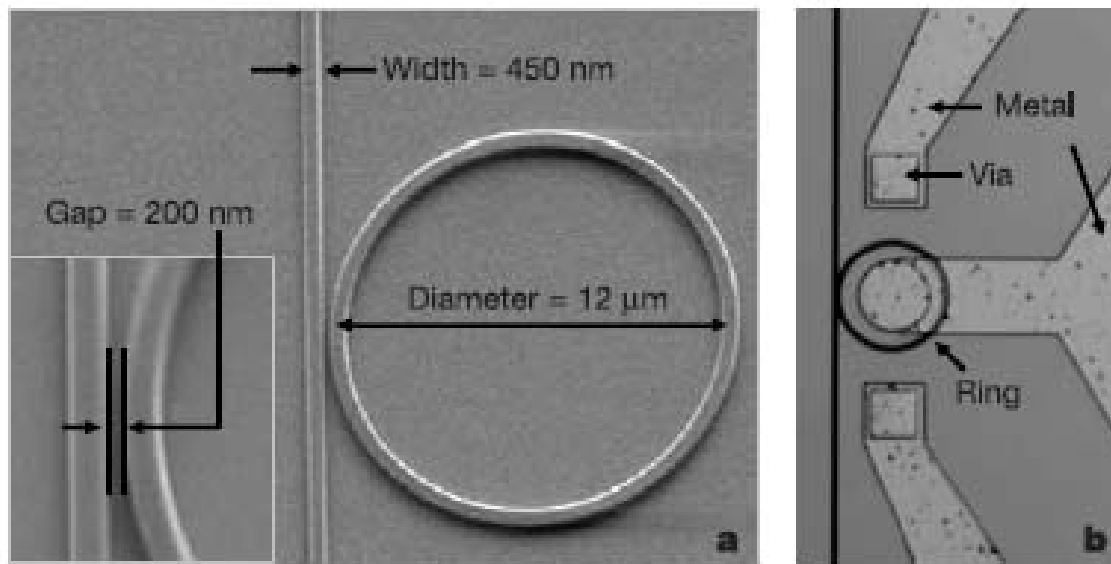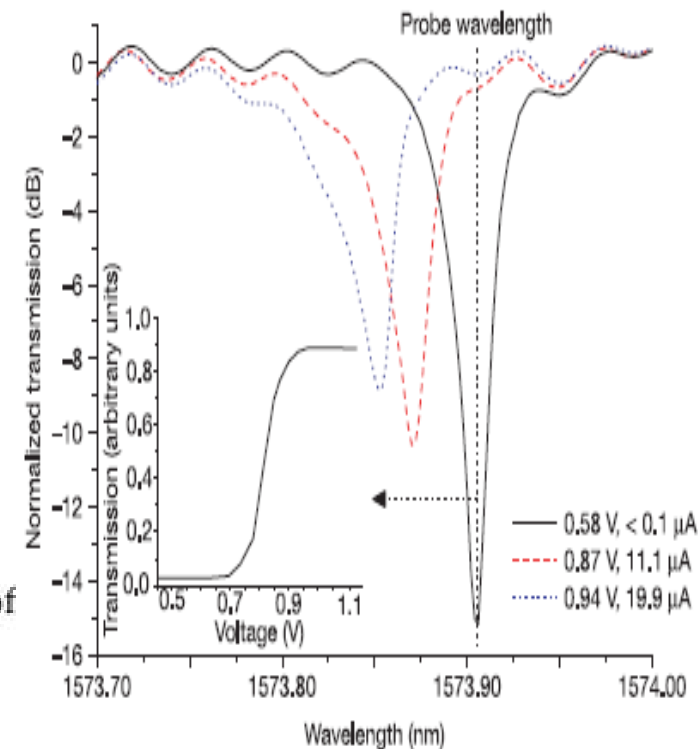
微腔光学滤波器：波分复用光通讯系统中对某一波长信号的下载.

Figure 2 | SEM and microscope images of the fabricated device. a, Top-view SEM image of the ring coupled to the waveguide with a close-up view of the coupling region. **b**, Top-view microscope image of the ring resonator after the metal contacts are formed. The metal contact on the central p-doped region of the ring goes over the ring with a 1-μm-thick silicon dioxide layer between the metal and the ring.
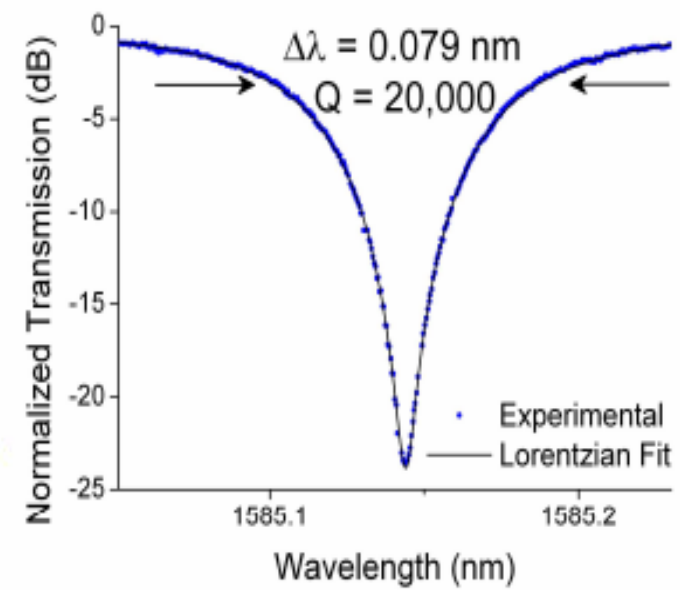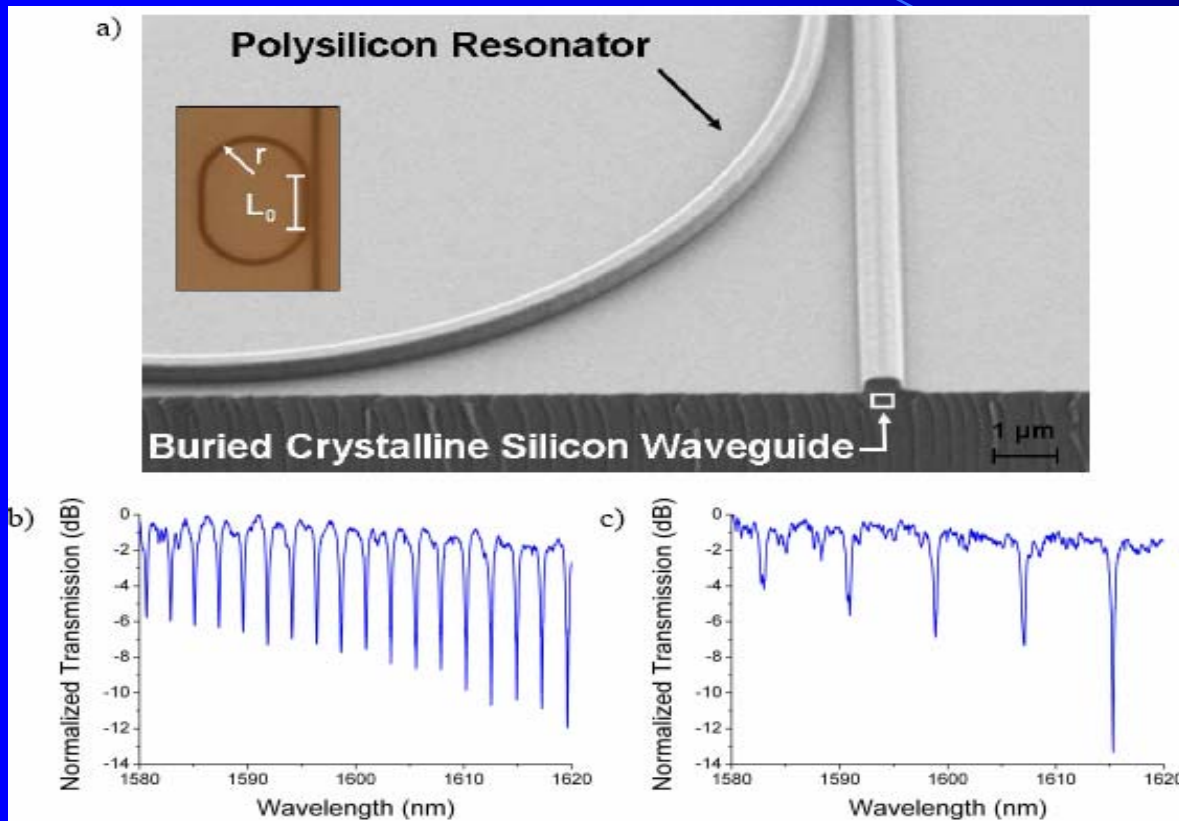
Fig. 5. Polysilicon racetrack resonators coupled to crystalline silicon waveguides. (a): Cross-section SEM of the structure before oxide cladding. Inset: Definition of r and coupling length L_0. (b) and (c): Quasi-TM polarized transmission as a function of wavelength for (b) r = 40 μm, L_0 = 3 μm and (c) r = 10 μm, L_0 = 5 μm.

通带(谐振)波长随环境的变化可作为一种非常敏感的传感器.

单光子测试

$$g^{(2)}(\tau) = <I(t)I(t+\tau)>/<I(t)>^2$$
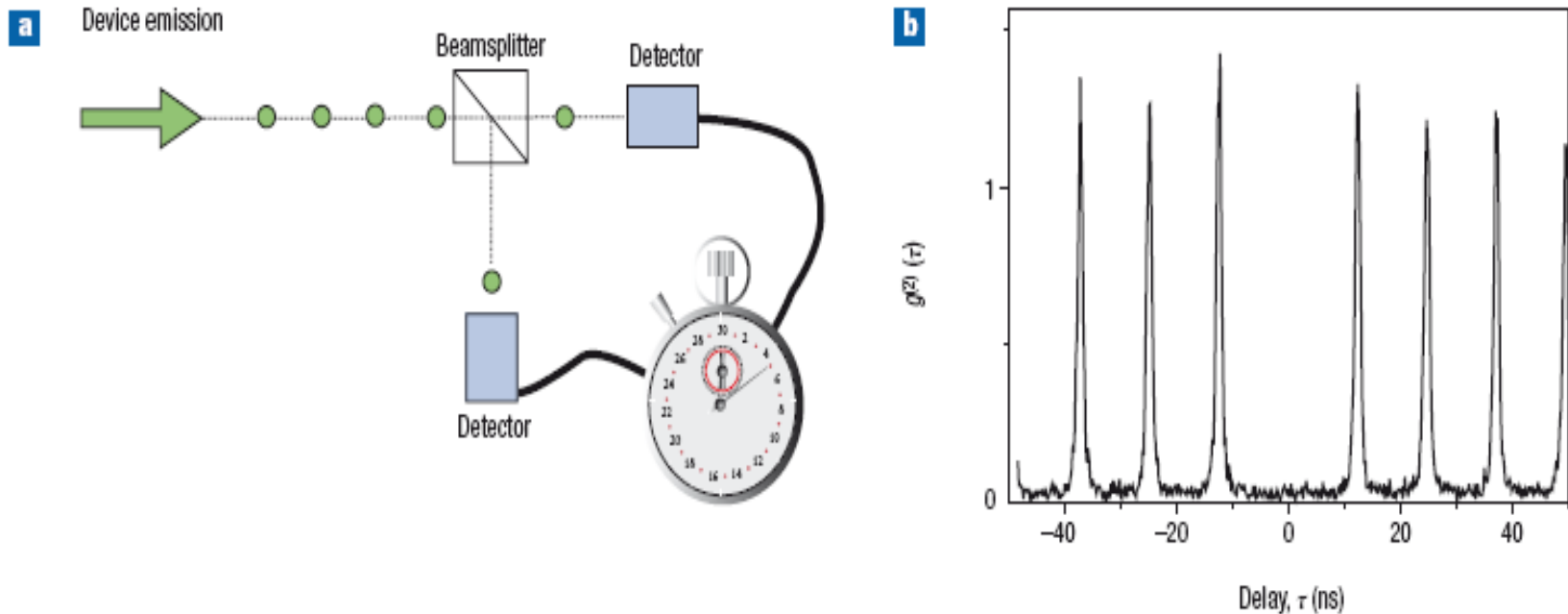
Box 1 Photon-correlation measurements

huang3

Figure B1 Measuring the correlation. **a**, Schematic of the set-up used for photon-correlation measurements. **b**, Second-order correlation function of the exciton emission of a single dot in a pillar microcavity. Reproduced with pemission from ref. 41. Copyright (2005) OSA.

huang3   yzhuang, 2008-3-6

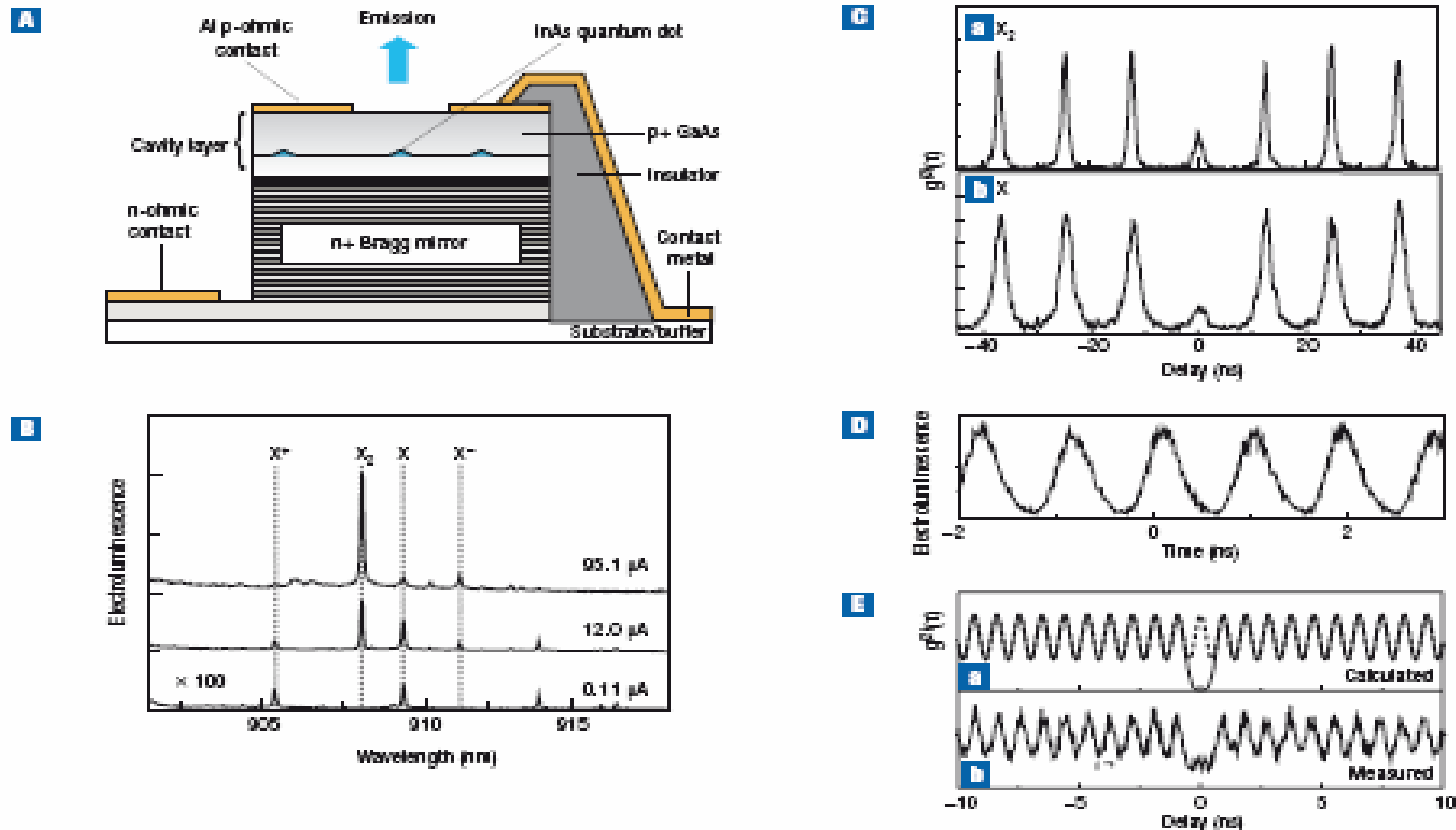# A. J. SHIELDS,"Semiconductor quantum light sources," Nature Photonics, vol.1, p.215(2007)

Figure 5 Electrically driven single-photon emission. A, Schematic of a single-photon LED. B, Electroluminescence spectra of the device. Notice the spectra are dominated by the exciton X and biexciton X_2 lines, which have linear and quadratic dependence on drive current, respectively. Other weak lines are due to charged excitons. C, Second-order correlation function recorded for the exciton (a) and biexciton (b) emission lines. D, Time-resolved electroluminescence from a device operating with a 1.07 GHz repetition rate. E, Modelled (a) and measured (b) second-order correlation function of the biexciton electroluminescence at 1.07 GHz. (Adapted with permission from ref. 71, copyright (2005) AIP; and ref. 73, copyright (2005) APS.)

单模、低阈值、窄线
宽、大自由谱域、高
速、可调谐

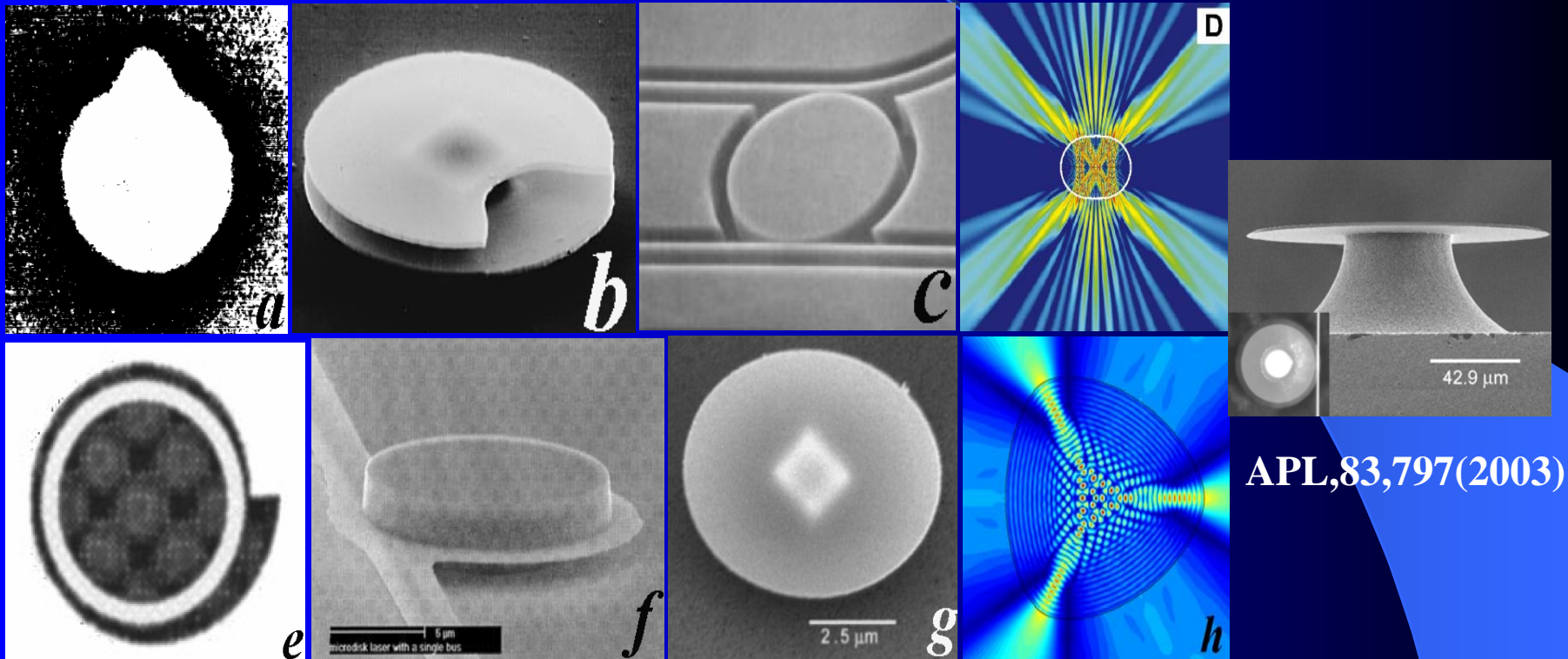**1，2，3** ⟷ **微腔**
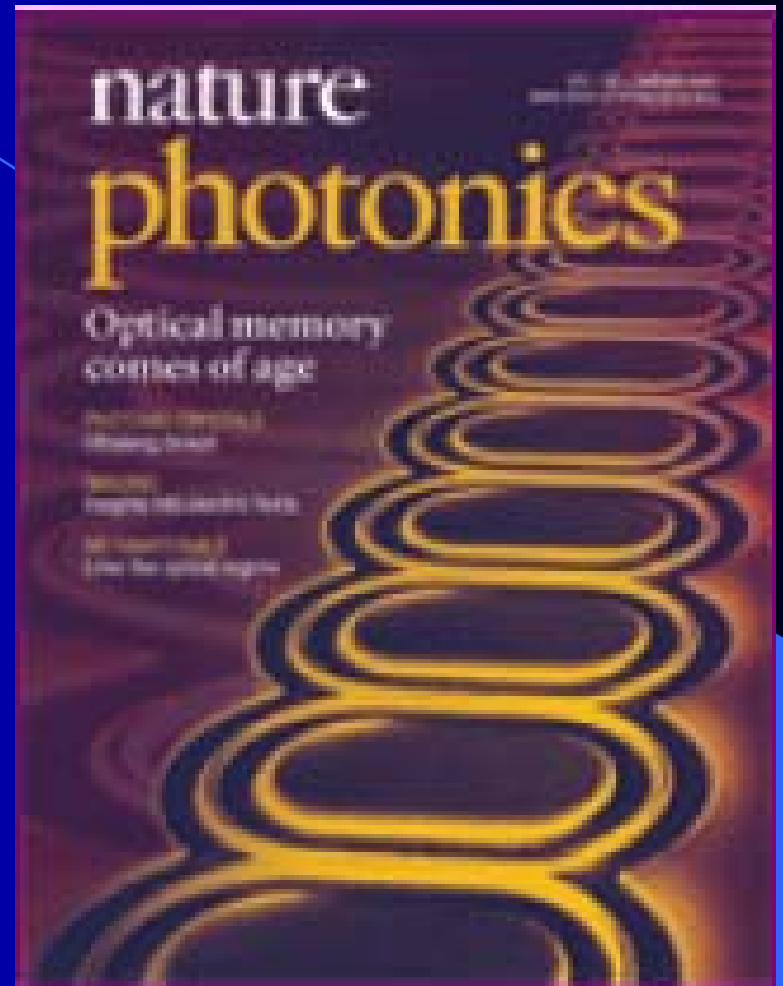
体积小、品质因子高

微腔激光器

微腔滤波器

微腔光开关

微腔调制器

本报告
重点

微腔传感器

……

Methods for obtaining directional emission

APL,83,797(2003)

Appl.Phys. Lett., (a)62, 561(1993), (b)65,3167(1994), (e)83, 1710(2003),(g)84, 861(2004); (c)J. Lightwave. Technol., 15, 2154(1997); (d) Science, 280, 1556(1998); (f) IEEE Photon. Technol. Lett., 15,1330(2003); (h) Phys. Rev. Lett., 93, 133902(2004)

圆环WG型光学微腔列阵
作为光速调控器件

S.-Y.Lee, "**Quasiscarred Resonances in a Spiral-Shaped Microcavity,**"
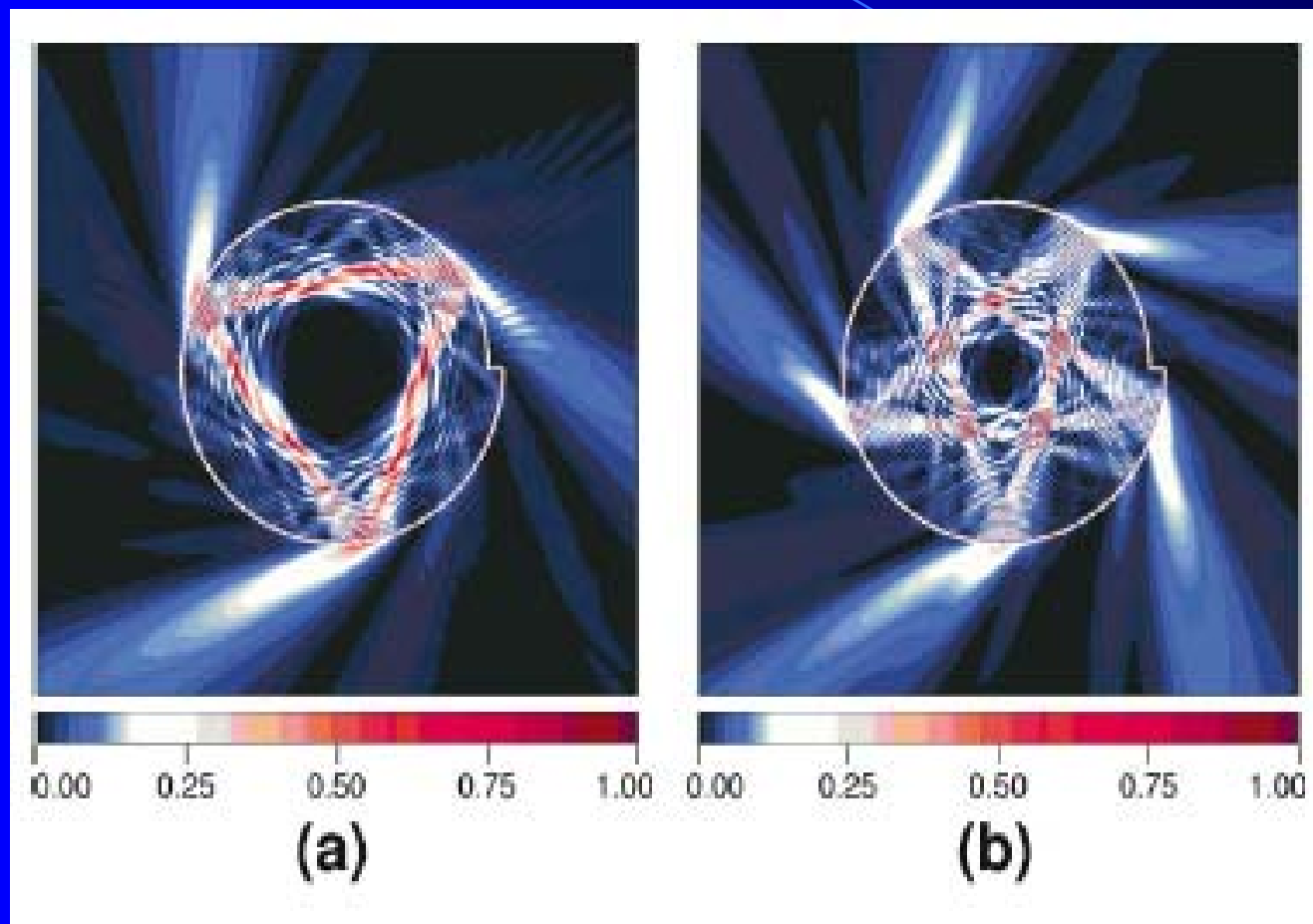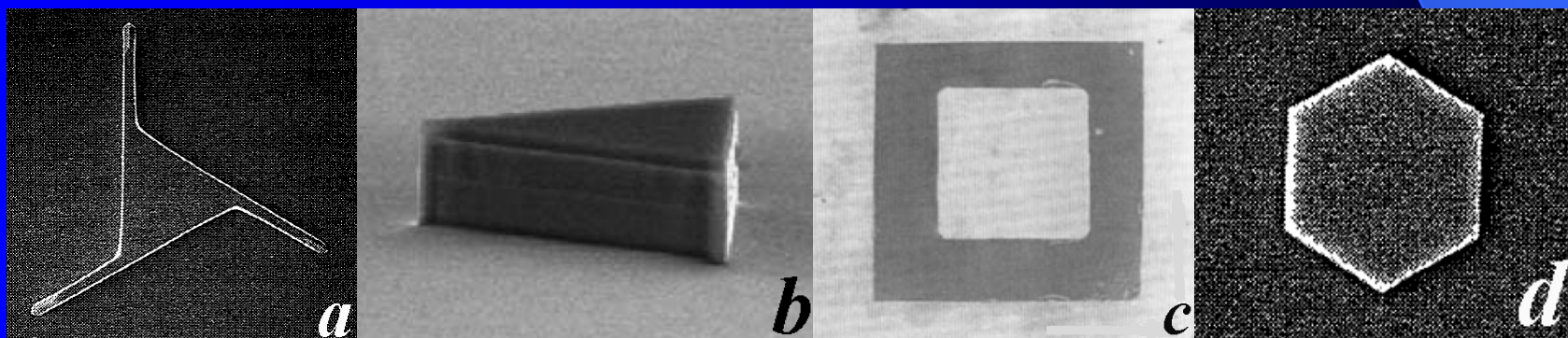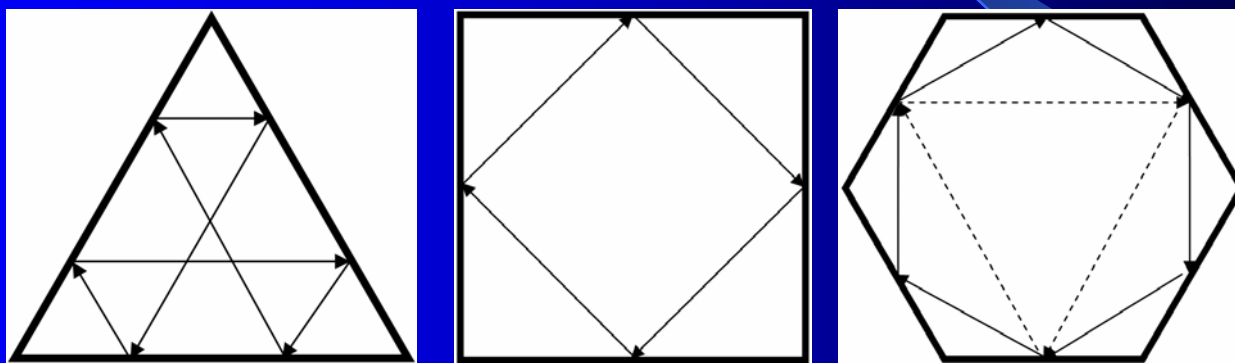Phys. Rev. Lett., vol.93, 164102(2004)

FIG. 3 (color). Field intensity plots of quasiscarred resonances in the spiral-shaped microcavity. (a) $n = 2$ **and** $nkR = (109.70, -0.1128)$**. (b)** $n = 3$ **and** $nkR = (109.59, -0.1127)$**. In figures, the field intensity is normalized by scaling the maximum intensity as one.**

huang5
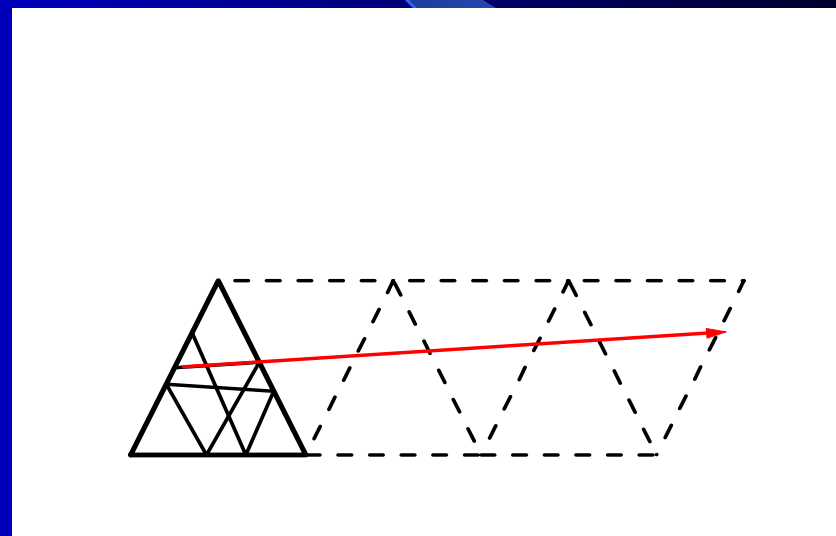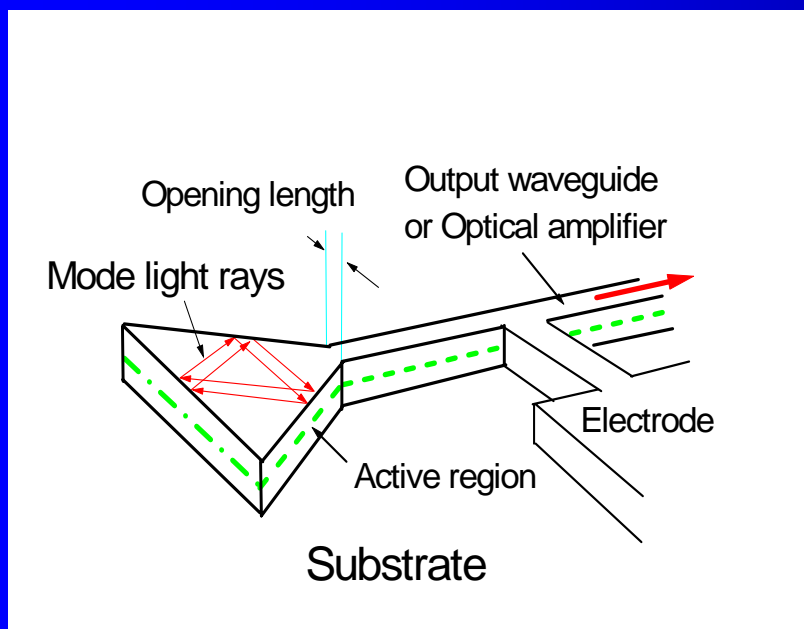
圆形腔优点：小体积，超高品质因子
　　缺点：定向输出困难，耦合长度短
多边形微腔激光器
正三角形腔、正方形腔、正六边形腔

II. Equilateral Triangle Resonators (ETR) Lasers

Special type of whispering-gallery cavity

Unfolding mode light ray, ETR is equivalent to a deformed Fabry-Perot cavity

Y.Z. Huang et al, IEEE J. Sel. Topics Quantum. Electron., vol. 12, pp.59-65(2006)

Transverse and longitudinal eigenvalue equation

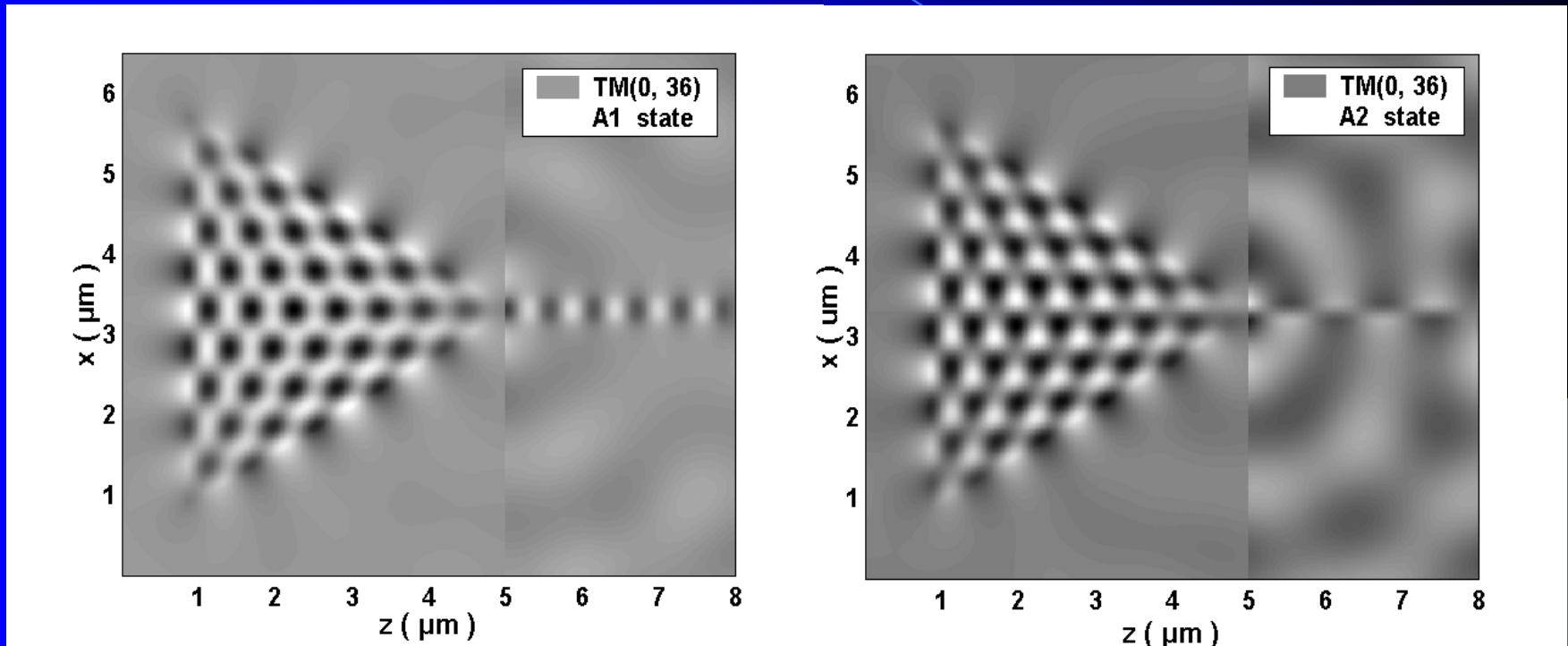$$\kappa_m \frac{\sqrt{3}\,a}{4} = \frac{(m+1)\pi}{2}$$

$$\beta_l \frac{3a}{2} + 3\varphi = 2l\pi$$

$$\varphi = 2\tan^{-1}\left(\frac{\sqrt{3}\,\beta_l\xi}{2\gamma\xi_1}\right) + \frac{1+(-1)^m}{2}\pi$$

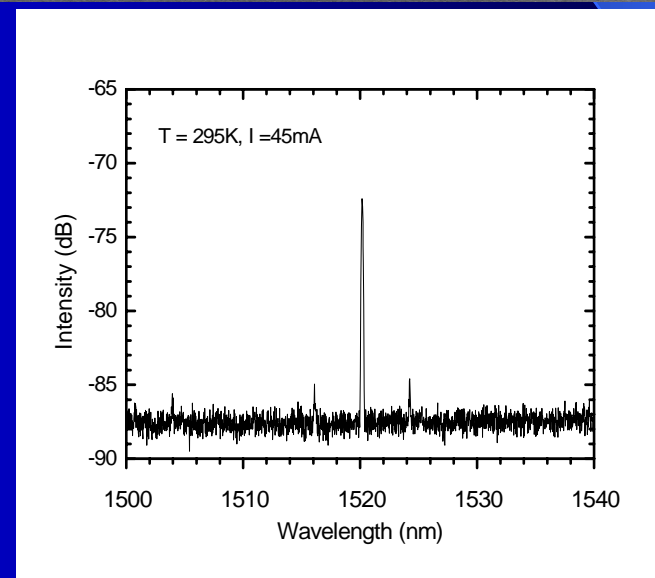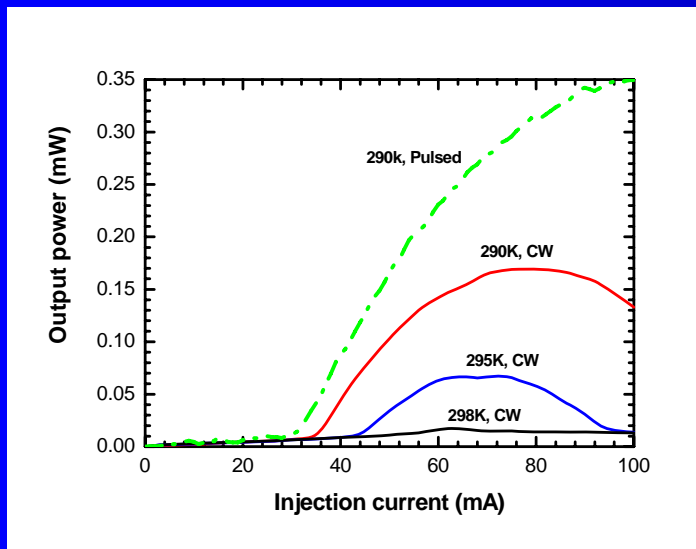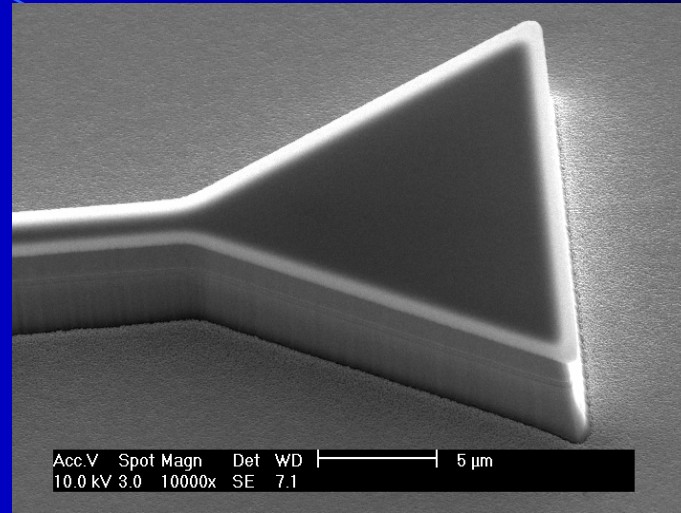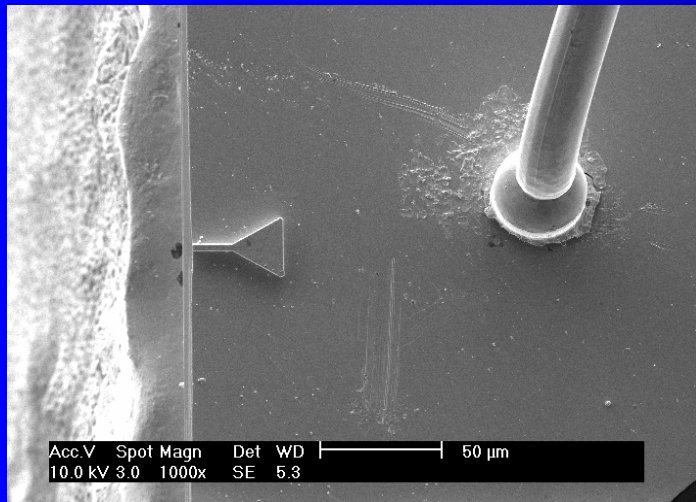l and m are longitudinal and transverse mode numbers, and mode wavelength is:

$$\lambda_{m,l} = \frac{3Na}{\sqrt{(2l - 3\varphi/\pi)^2 + 3(m+1)^2}}$$

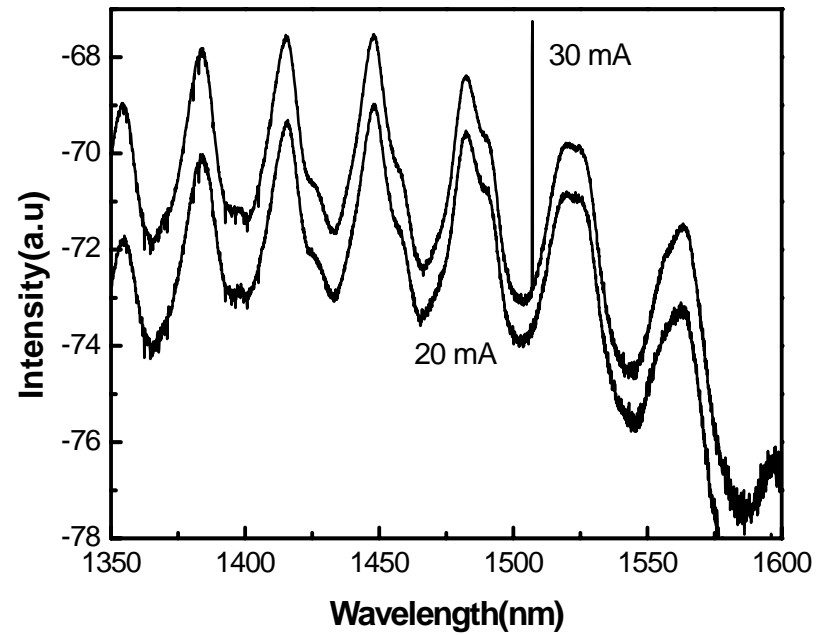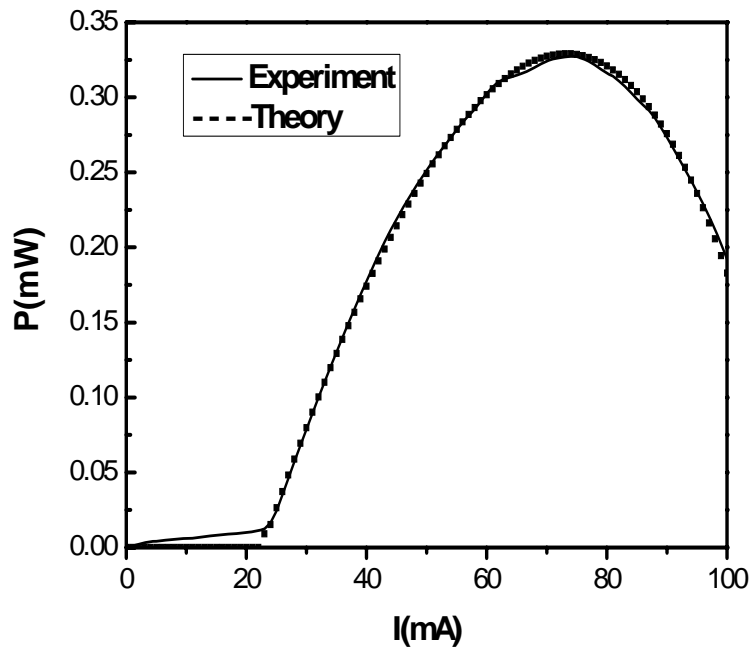# Mode field intensity for an ETR lasers with output waveguide obtained by FDTD simulation

The side-length and inner refractive index of ETR is 5μm and 3.2 respectively. The width of output waveguide is 0.3μm. The field intensity in the region of $z > 5$μm is magnified 5 times.

Directional Emission ETR laser with side length of 20 μm

Y. Z. Huang et al, IEEE Photo. Technol. Lett., 19, 953(2007)
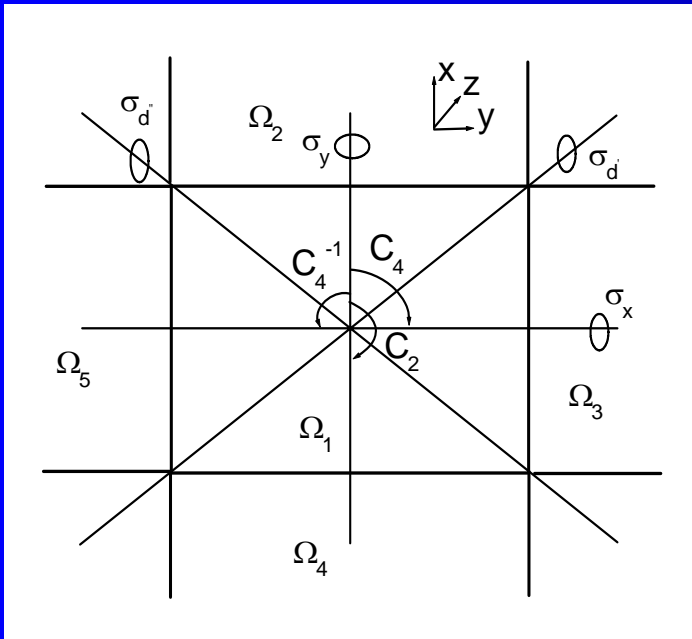
边长10 μm的正三角形微腔激光器输出功率-电流关系及输出光谱，295K电注入连续激射.

III. Mode Confined in Rectangular Microresonator

1. Modes confined in square resonator with mode indices (*p,q*) denoting the numbers of wave nodes in the *x* and *y* directions

Mode field patterns:

$$F_{zp,q} = F_{zxp}(x)\, F_{zyq}(y)$$

W. H. Guo, et al, **IEEE J. Quantum Electron., vol. 39, p.1563 (2003);**

Y. D. Yang, et al, IEEE J. Quantum Electron., vol. 43, p.497(2007)

Mode field distribution and eigenvalue equations:

$$F_{zx}^p = \begin{cases} \cos(\kappa_x x - \varphi_x) & |x| \leq a/2 \\ \cos(\kappa_x a/2 - \varphi_x)\exp[-\gamma_x(x - a/2)] & x > a/2 \\ \cos(-\kappa_x a/2 - \varphi_x)\exp[\gamma_x(x + a/2)] & x < -a/2 \end{cases}$$

$$F_{zy}^q = \begin{cases} \cos(\kappa_y y - \varphi_y) & |y| \leq b/2 \\ \cos(\kappa_y b/2 - \varphi_y)\exp[-\gamma_y(y - b/2)] & y > b/2 \\ \cos(-\kappa_y b/2 - \varphi_y)\exp[\gamma_y(y + b/2)] & y < -b/2 \end{cases}$$

$$\kappa_x^2 + \kappa_y^2 = n_1^2 k_0^2 \qquad \kappa_v^2 + \gamma_v^2 = (n_1^2 - 1)k_0^2$$

$$\kappa_x \tan(\kappa_x a/2 - \varphi_x) = \eta \gamma_x$$
$$\kappa_y \tan(\kappa_y b/2 - \varphi_y) = \eta \gamma_y$$
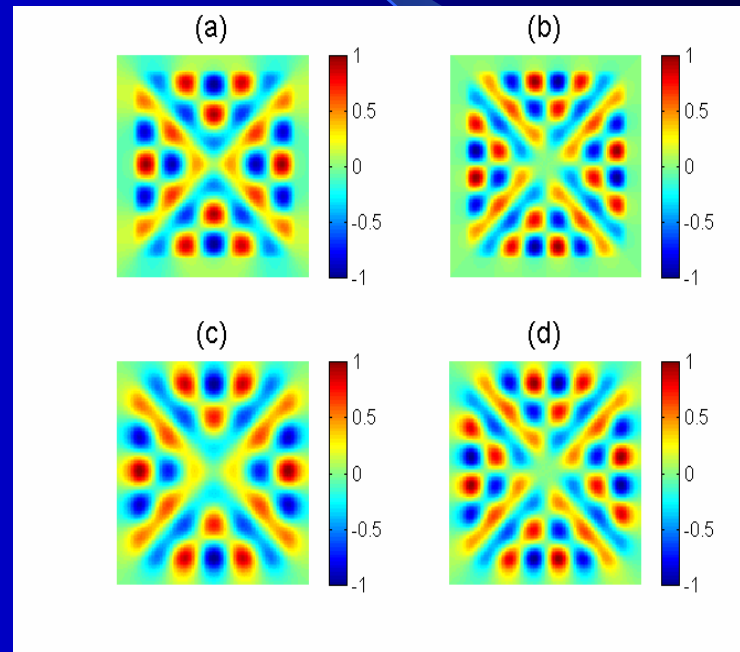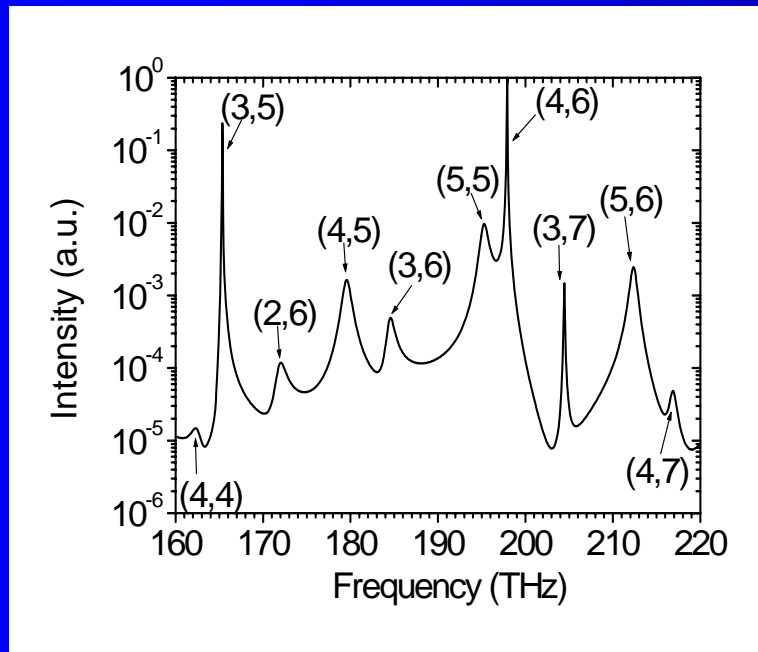
$\eta = n_1^2/n_2^2$ **for TE mode**
$\eta = 1$ **for TM mode,** $v = x, y$

The total internal reflection limits the difference between k_x **and** k_y, $\varphi_v = 0$
or $\pi/2$ **as the corresponding** *p* **or** *q* **is even or odd number, respectively.**

Mode intensity spectrum obtained by FDTD simulation and Pade approximation for a square resonator with sidelength of 2μm and *n*=3.2
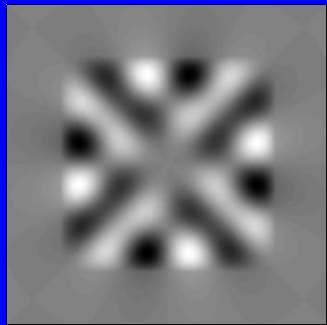
TE0,14   TE0,16

FDTD
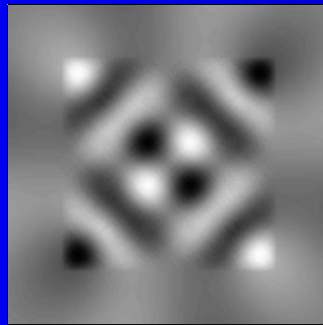
Analytical

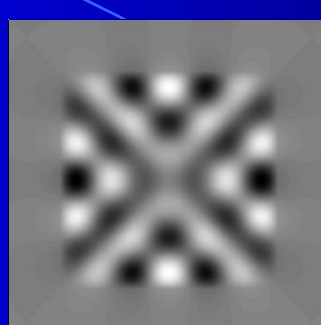Mode with same symmetry in x and y directions have high Q-factor.

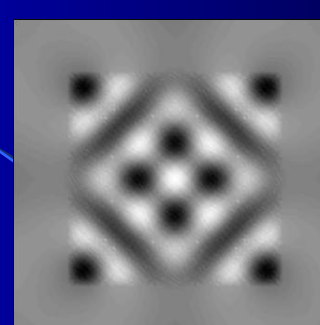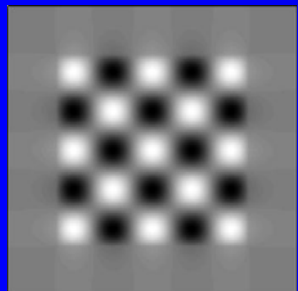# Mode field patternin a square resonator with $a = 2\mu$m and n=3.2.

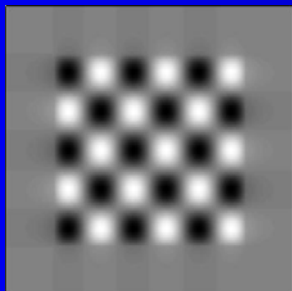TE^o(3,5)   TE^e(3,5)   TE^o(4,6)   TE^e(4,6)
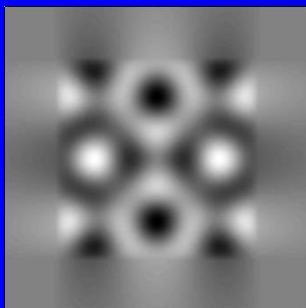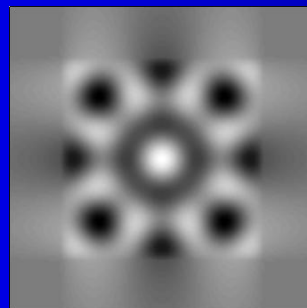
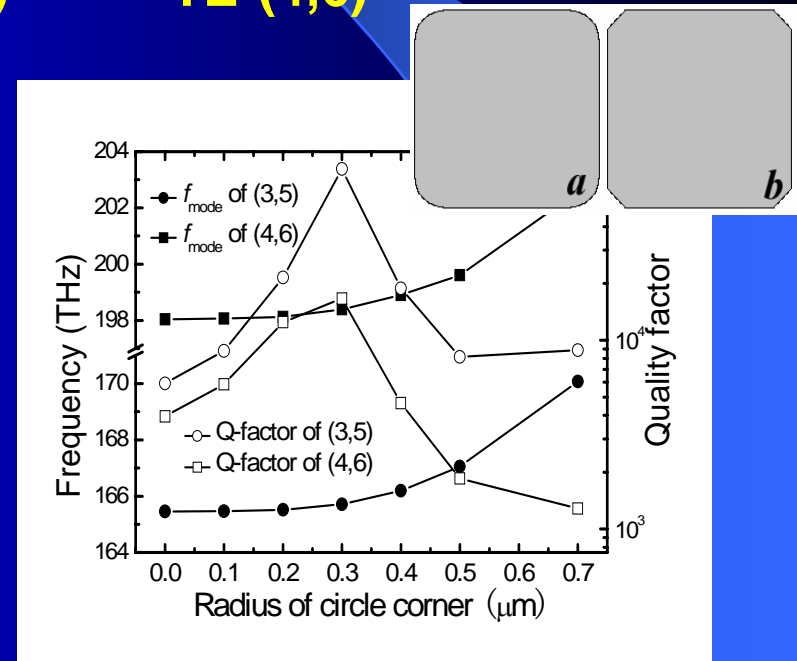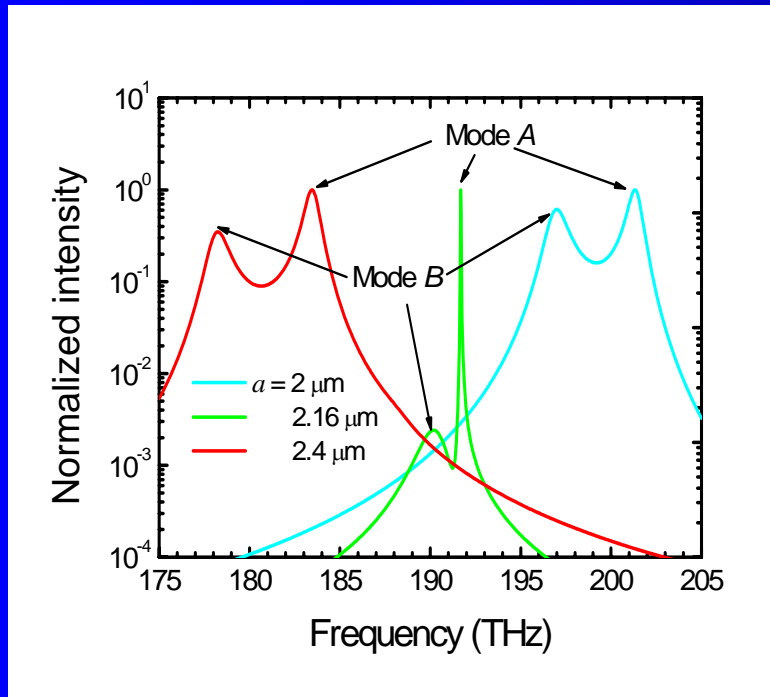TE(4,4)   TE(4,5)   TE(3,6)

TE^o(2,6)   TE^e(2,6)
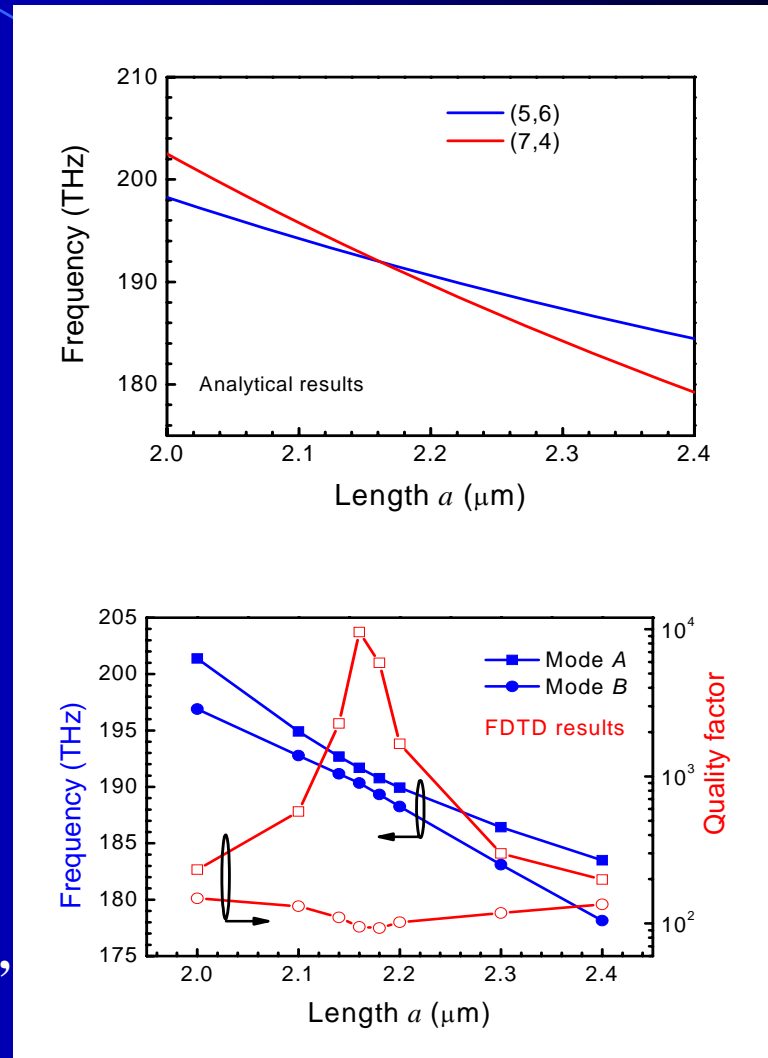
Mode Q-factors even increase in a square with circular corners.

High Q-factor modes result from mode coupling between two degenerate modes with the same symmetry.
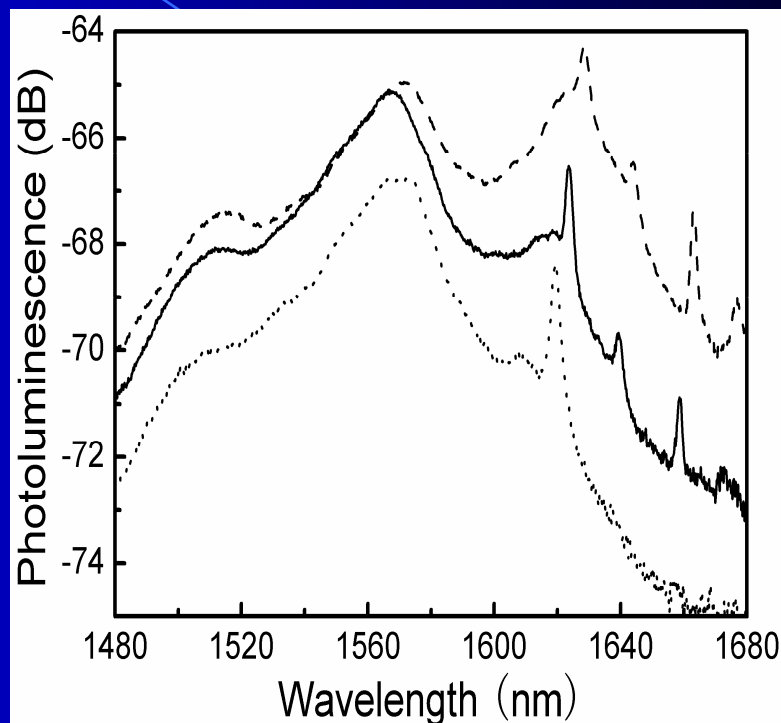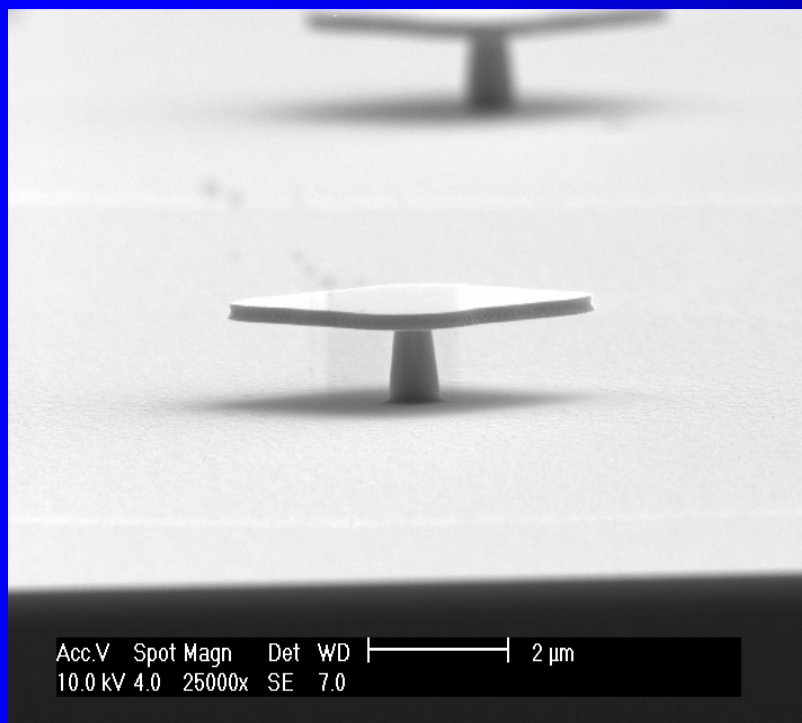

$b = 2 \mu$ m and n=3.2

Y. D. Yang, et al, IEEE J. Quantum Electron., vol. 43, p.497(2007)

Similar results published by J. Wiersig in Phys. Rev. Lett., vol.97, 253901(2006).
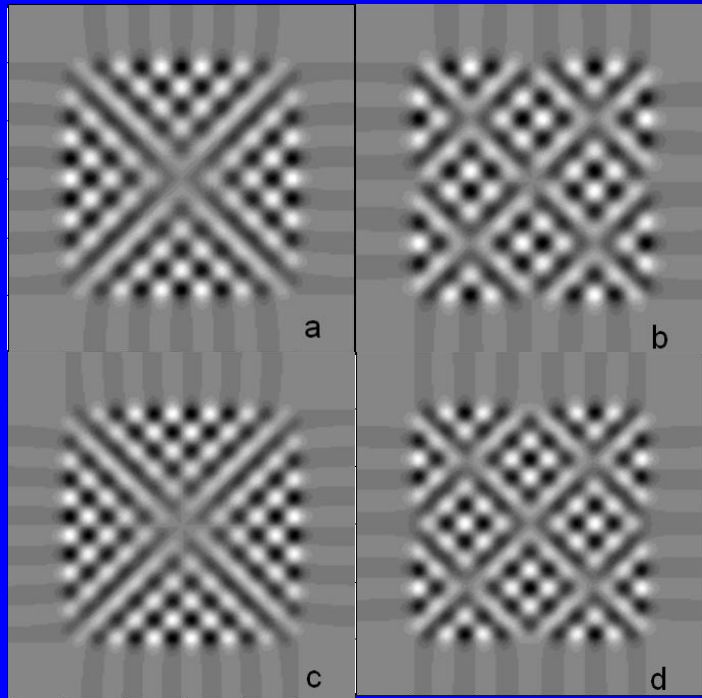
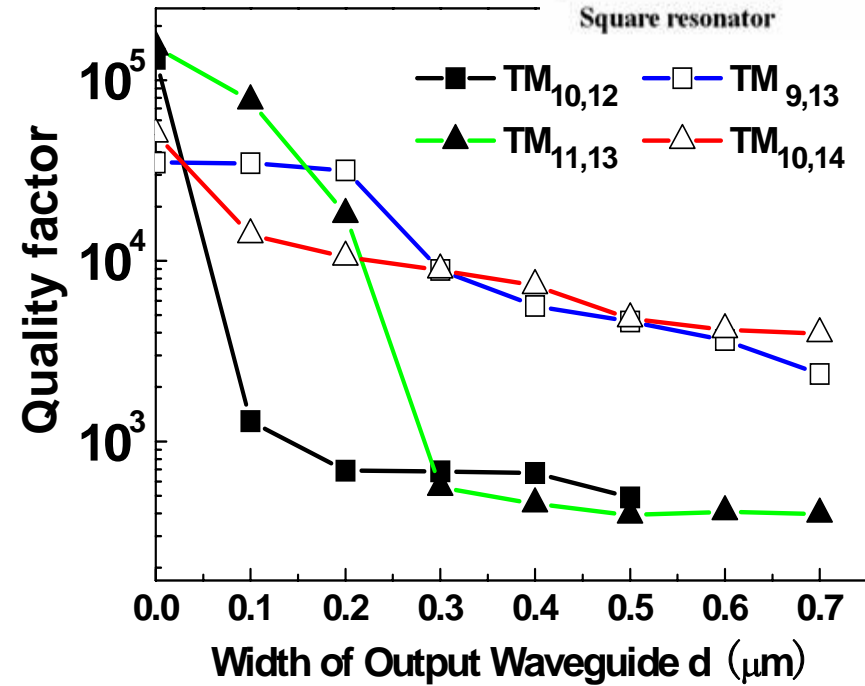# Square resonator fabricated by selected chemical etching technique.

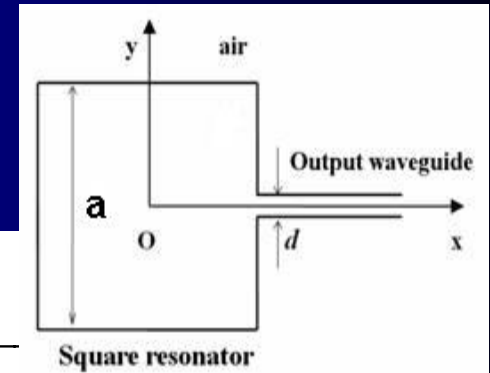**SEM picture and photoluminescence of a square with side length of 7 μm.**

Y. Z. Huang et al, IEEE Photon. Technol. Lett., vol. 17, p.2589(2005)

Directional emission for square microlasers

Field distribution of (a)TM$_{10,12}$, (b)TM$_{9,13}$, (c) TM$_{11,13}$, (d) TM$_{9,13}$ in a square with sidelength of 4 μm and refractive index 3.2.

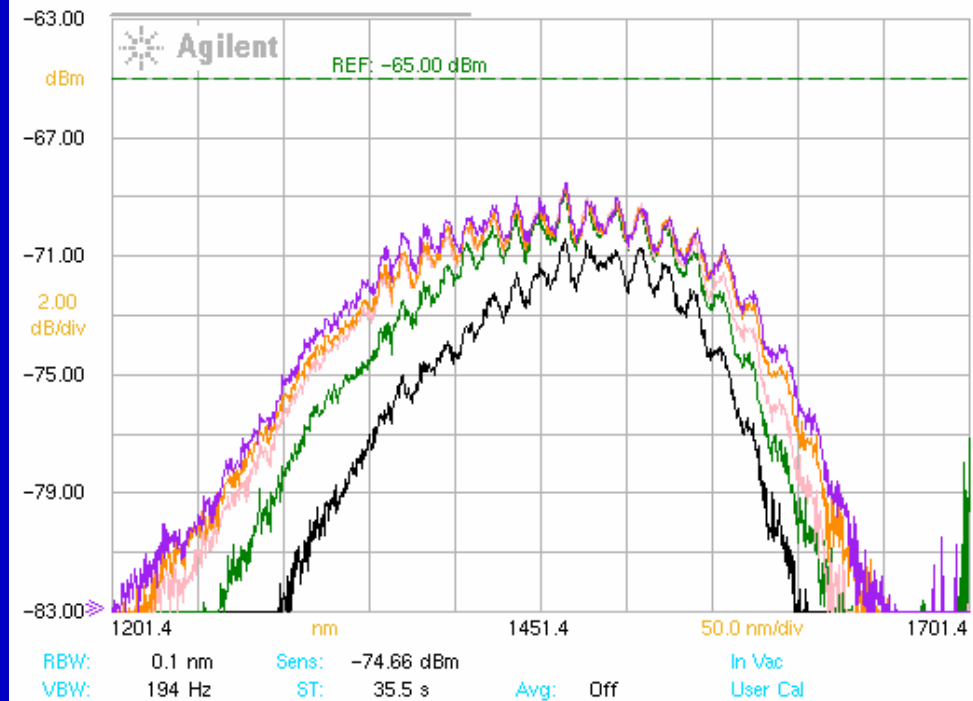**Mode Q-factor versus width of output waveguide**

Directional Emission square InGaAsP laser with 20 μm side.

Output spectra at room temperature
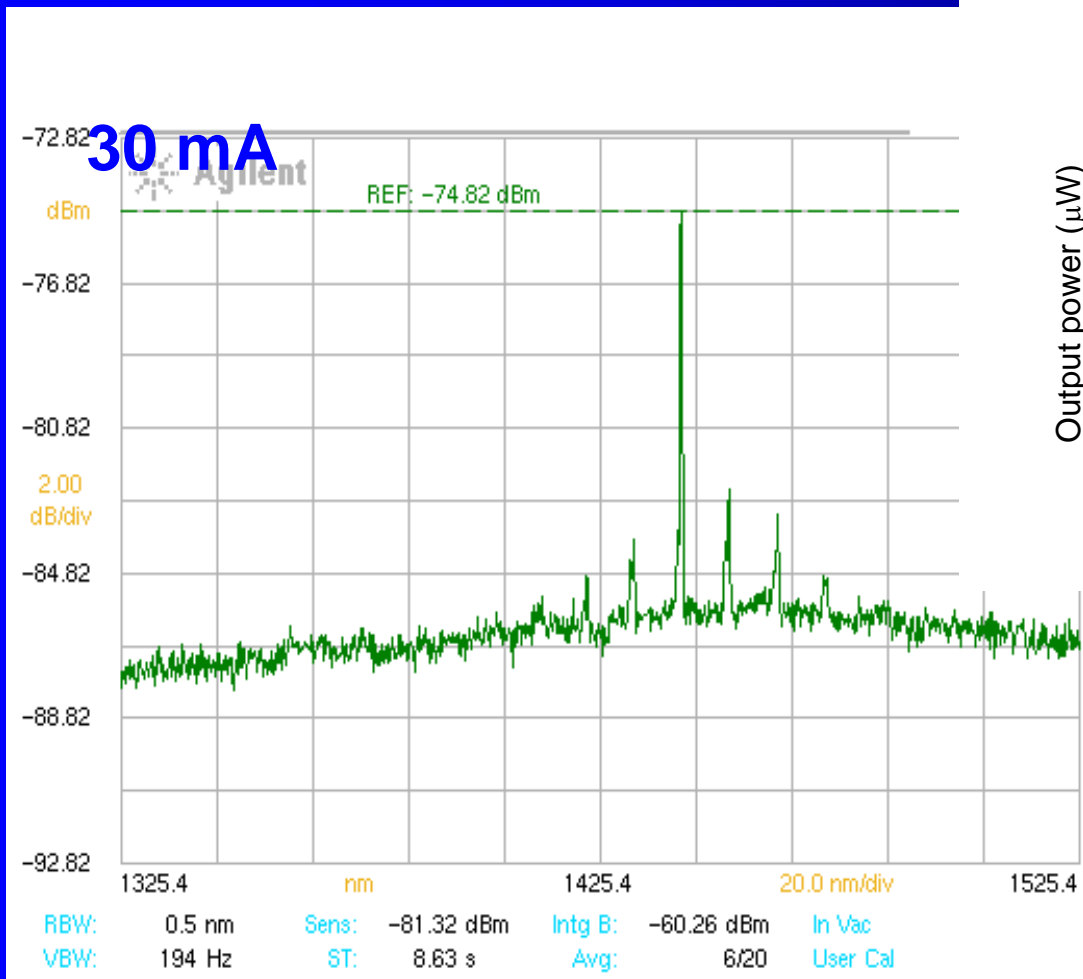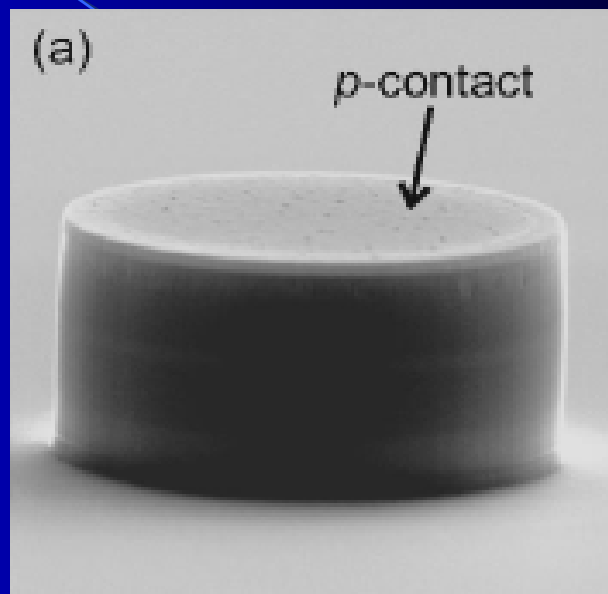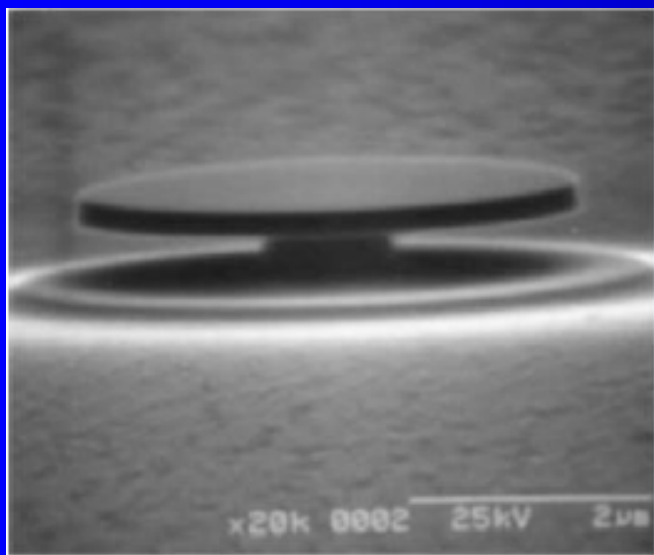

First run. CW electrically operation is realized at 200K.

Derivative resistor is one order larger than the ETR laser. (70~80 Ω)

Laser spectrum and output power-injection current curve of a InGaAsP/InP square laser with side length 20μm at 200K.

四．纵向弱波导三维微腔中的高Q值TM模

(a) p-contact

x20k 0002 25kV 2μs

传统的选择性腐蚀形成的强
折射率波导结构微盘激光器.
不利于电注入和散热

能否在纵向为半导体弱波导的三维微腔中得到高Q值模式？

Whispering-Gallery Modes (WGMs) in 3D microcylinder

TE and TM modes in 3D microcylinder → How to get High-Q modes in microcylinders ?

Vertical radiation loss

3D finite difference time-domain (FDTD) simulation under circular symmetry→2D case

parameters $R = 1$ μm, $d = 0.2$ μm, $n_1 = 3.4$.

TE (TM) modes: magnetic (electric) field H_z (E_z) is symmetry to r-Φ plane.

→Mode Q-factor versus the refractive index of cladding layer n_2

半径**1μm**的纵向折射率及厚度为**n2/n1=3.4, d=0.2 μm /n2**的对称圆柱微腔中**TE**和**TM**模**Q**值及模式波长随**n2** 变化。 TM模波长对应的纵向传播及辐射模式不存在，因此在纵向弱限制光学微腔中TM模可具有高Q值。

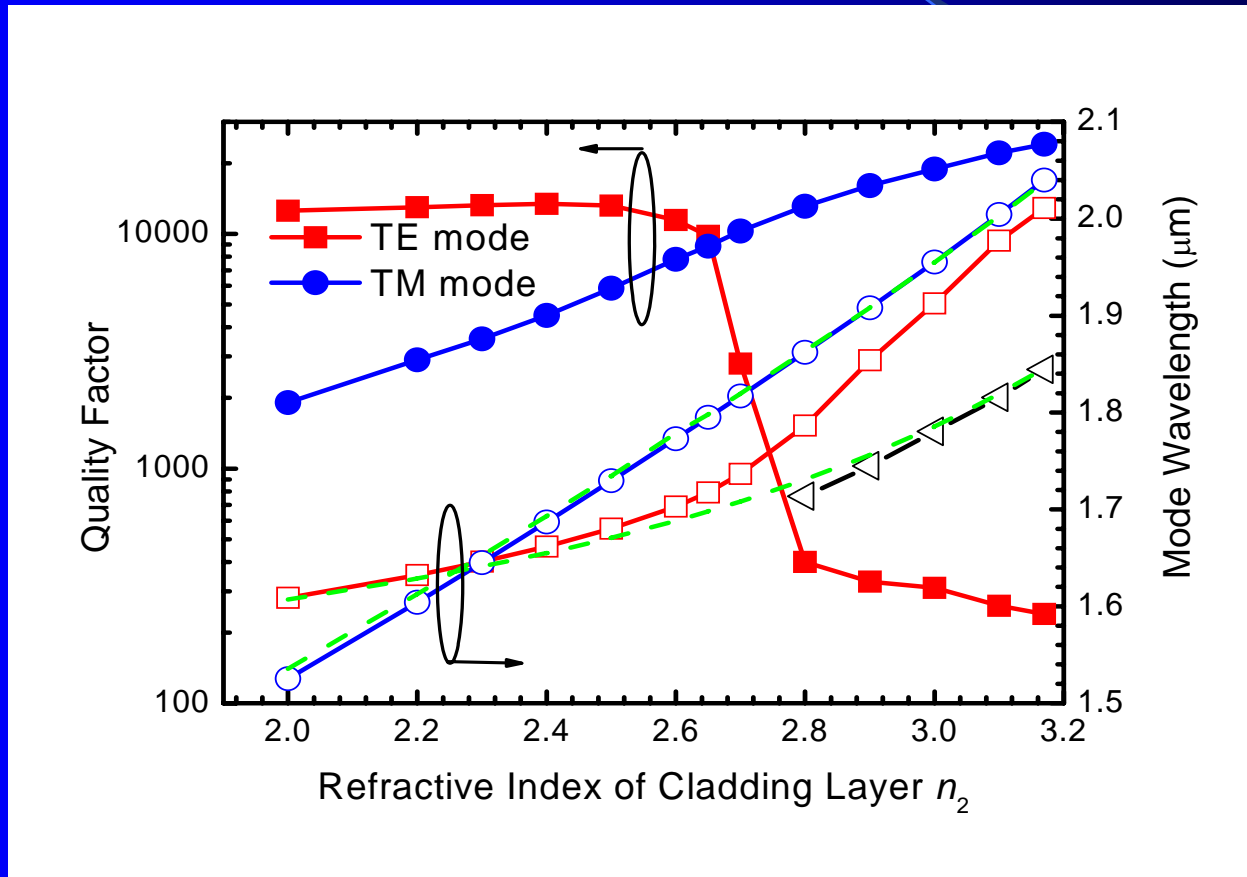**Y. D. Yang, et al, Phys. Rev. A, vol.75, 013817 (2007)**

The Q-factor of the mode marked by triangle is less than 1000.

Dashed green lines are mode wavelength of the WGMs obtained from eigenvalue equation of 2D problem under effective index approximation.

Mode wavelengths of the WGMs under effective index approximation and cut-off wavelength of the same order radiation modes in the cladding layers obtained by the following eigenvalue equation:

$$J_v(knR)H_v^{(2)'}(kR)=$$
$$\eta\ J_v'(knR)\ H_v^{(2)}(kR)$$

(M. Hentschel et al, Phys. Rev. E66, 056207 (2002))

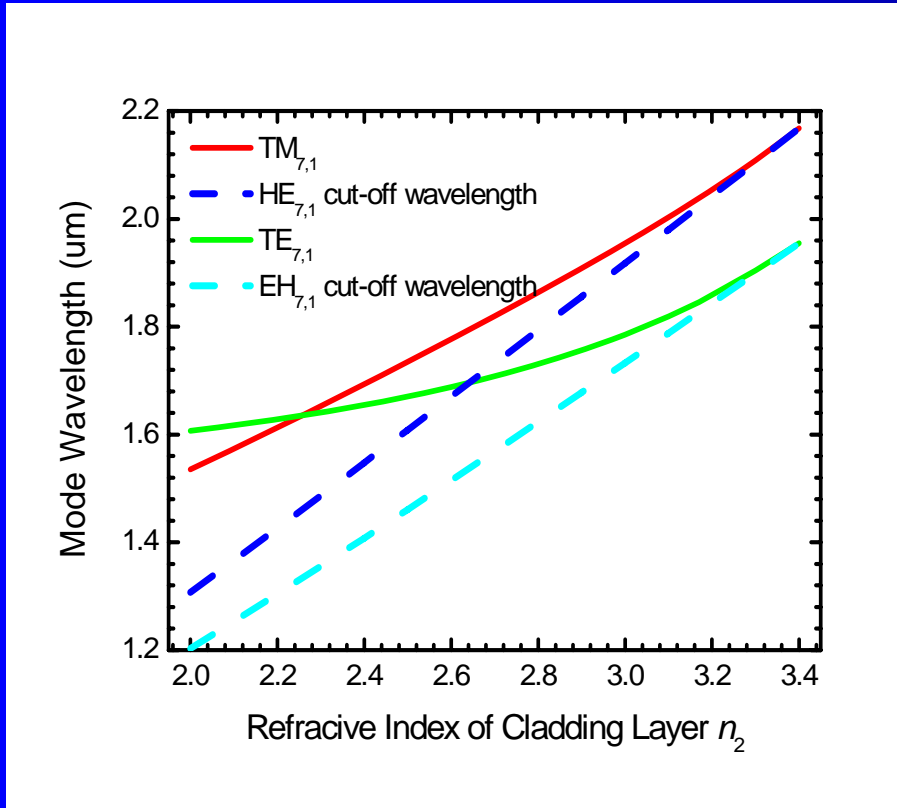$n=n_{eff}$ for TE and TM WGMs
$n=n2$ for HE$_{off}$ and EH$_{off}$
radiation modes
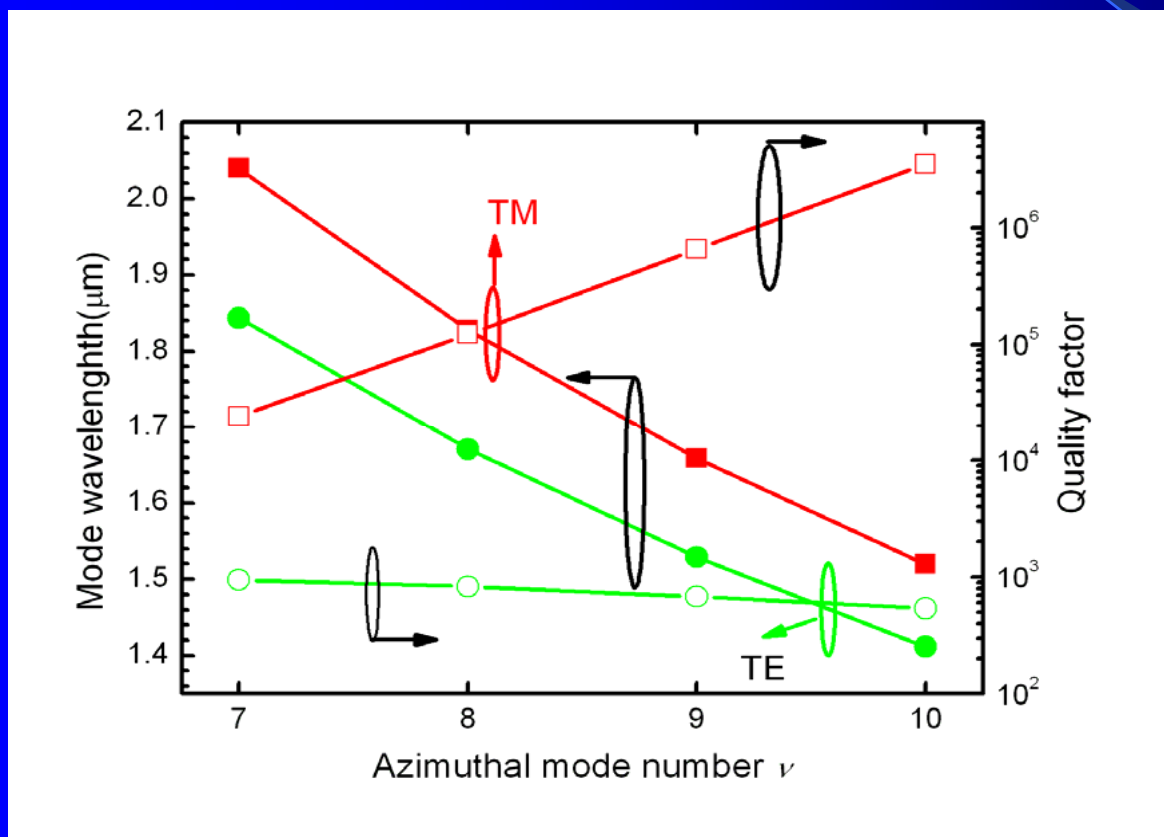$\eta =n$ for TM and HE*off* modes
$\eta =1/n$ for TE and EH*off* modes

三维圆柱型波导中横磁场模式波长大于同阶横电场及辐射模式波长 (*R = 1* μm, *d = 0.2* μm, *n2/ 3.4/n2*)

When n_2>2.65, λ $_{WGM}$(TE$_{7,1}$)< λ $_{radiation}$(HE$_{7,1}$)*off* → vertical radiation loss

Mode wavelengths and Q-factors of TE and TM WGMs versus azimuthal mode number obtained by FDTD simulation for the microcyliner with vertical refractive indices 3.4/3.17.

TE WGMs:
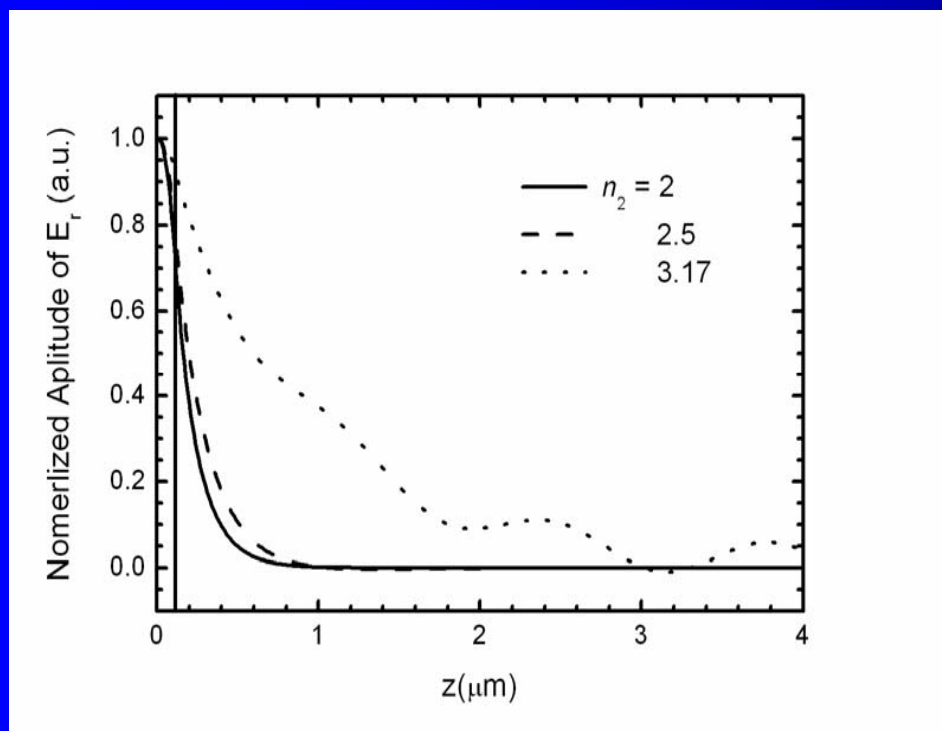$Q \sim 10^2$
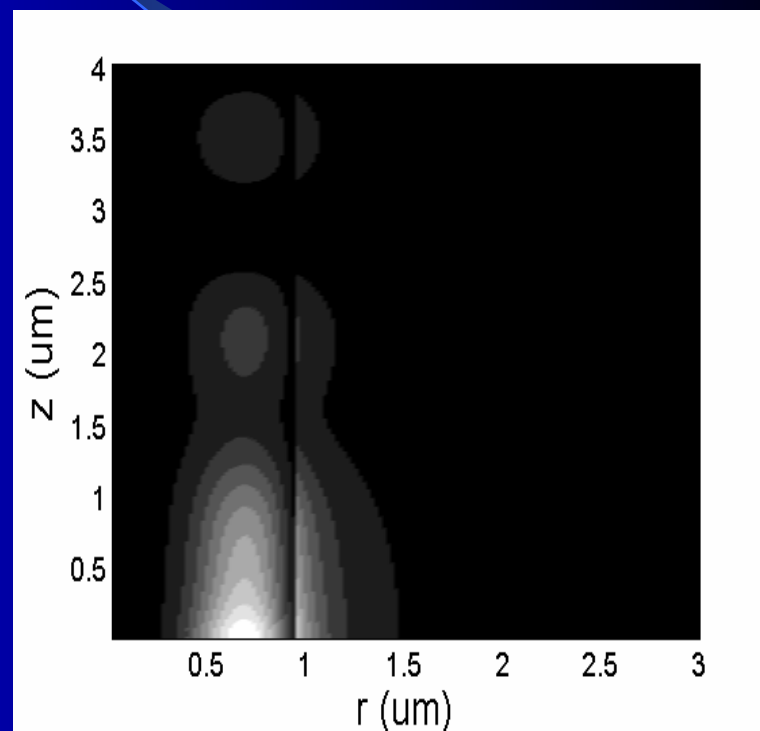
TM WGMs:
$Q \sim 10^4 \rightarrow 10^6$

FDTD 模拟 得到的TE模和TM模的Q值和波长随角波数v的变化

Vertical field distribution of TE$_{7,1}$ WGM at n$_1$ = 3.4 and n$_2$= 2, 2.5, and 3.17 obtained by FDTD simulation.
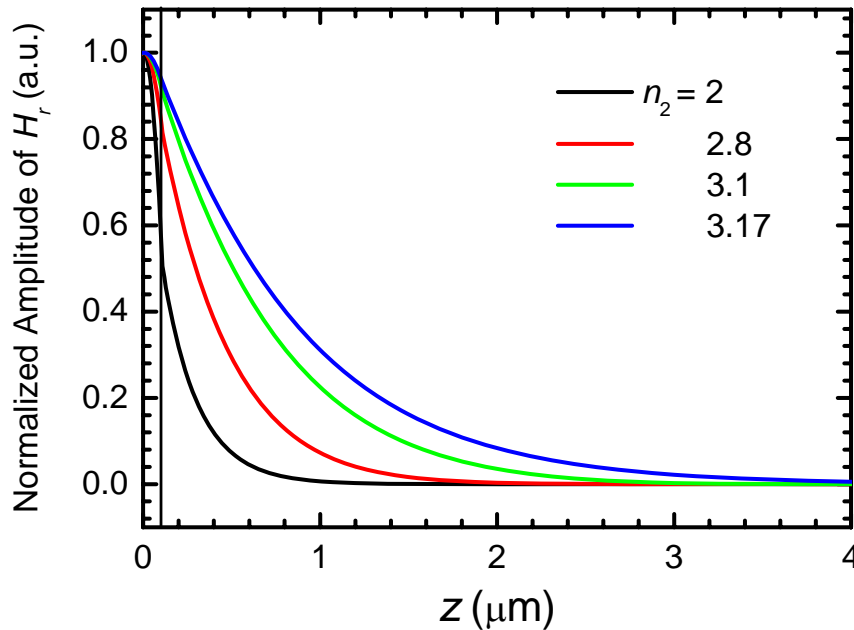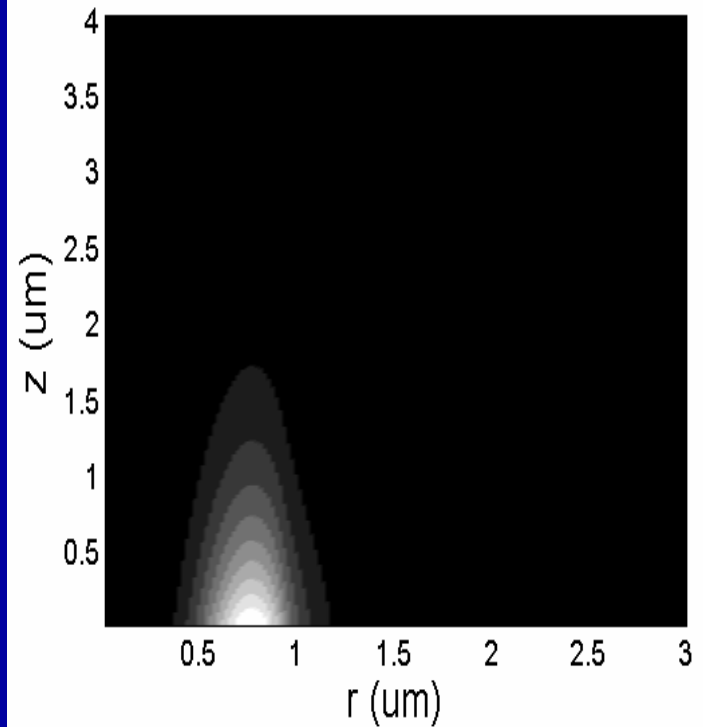

$r = 0.84R$

$n_2 = 3.17$

Vertical field distribution of $TM_{7,1}$ WGM at $n_1 = 3.4$ and $n_2 = 2, 2.8, 3.1,$ and 3.17 obtained by FDTD simulation.
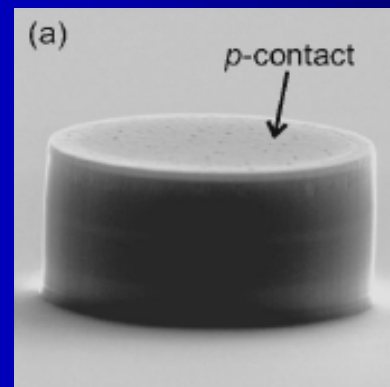

$r = 0.84R$

$n_2 = 3.17$

Mode wavelengths of WGMs and radiation modes for microcyliner with vertical refractive indices 3.4/3.17

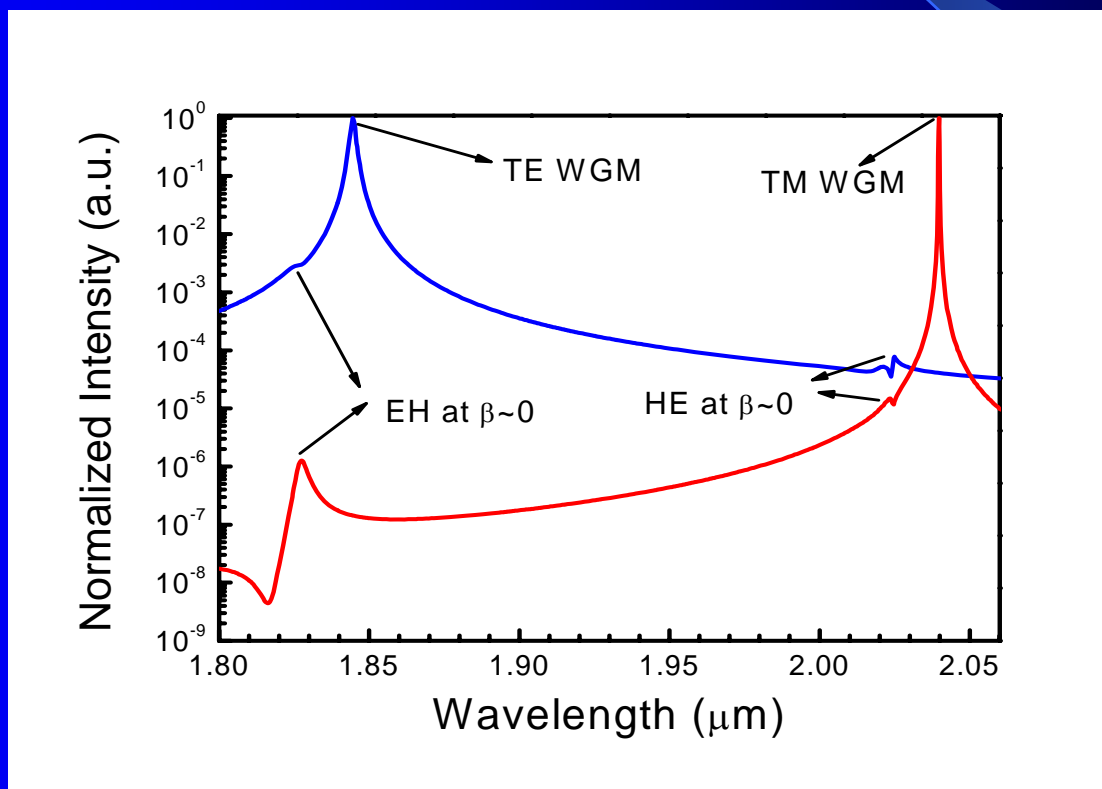| R (μm)	1.0	2.0	3.0	4.0	5.0	6.0
Mode index	9	21	33	45	58	70
λ -TM WGM (μm)	1.658	1.589	1.584	1.586	1.565	1.574
λ -TE WGM (μm)	1.532	1.533	1.548	1.560	1.546	1.558
λ (HE_{off}) (μm)	1.641	1.572	1.566	1.569	1.548	1.556
λ (EH_{off}) (μm)	1.511	1.511	1.526	1.539	1.527	1.537
Q (TE)	680	470	580	870	$\sim 10^4$	$\sim 10^6$

T. Baba et al, IEEE Photon. Technol. Lett., 9, 878(1997): GaInAsP micodisk lasers with radius 1→ 5 μm.

(a) p-contact
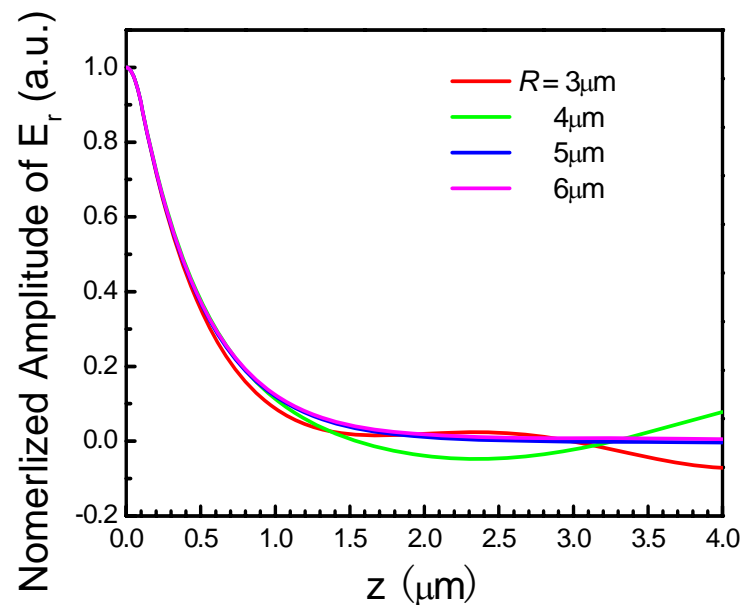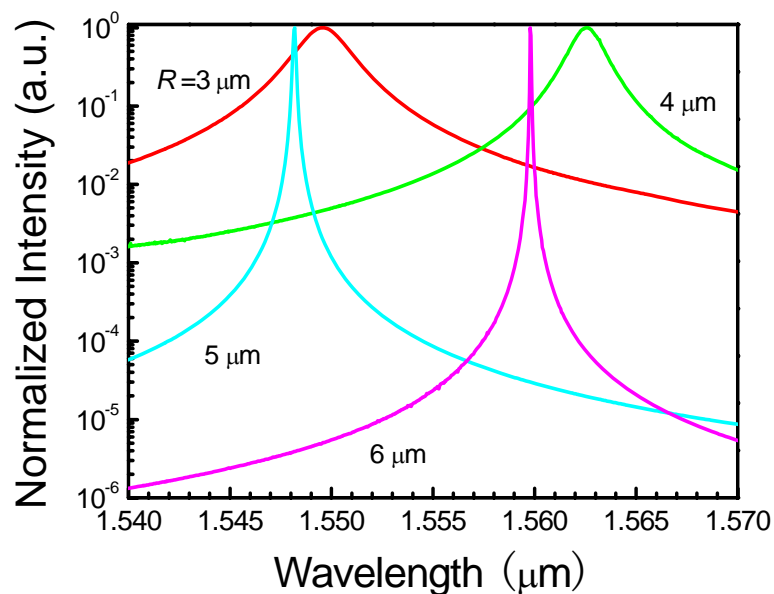
M. Arzberger et al, Appl. Phys. Lett., 79, 1766 (2001):In(Ga)As Quantum dot(well) microcylinder lases down to radius 5μm

(>7 μm)

三维WG微腔中,TM偏振的WGM波长总比对应的纵向辐射模波长大,不会造成纵向辐射损耗,而TE偏振的WGM则不然,而传统的材料总是倾向于支持TE偏振的模式,因此需要纵向折射率强限制,采用TM偏振的应变材料,则可研制结构简单的利于电注入和散热的WG型微腔激光器及单光子源.

FDTD模拟得到的**TE**和**TM**偏振**WGM**以及对应圆柱中辐射模**EH**和**HE**的模谱.

TE WGM的模式谱及纵向光场分布随圆盘半径的变化.

发现在纵向为半导体限制的圆柱形微腔中**TM**模的纵向辐射损耗基本为零,而**TE**模则只在半径大于**5~6 μm**,纵向辐射损耗才接近为零,提出一种研制高性能微腔激光器及单光子源的方案.

Phys. Rev. A Vol.75 013817 (2007)
IEEE Photonics Technology Letters 19, 1831(2007)

五. 结论

- 采用平面工艺研制的室温连续激射定向输出等边三角形激光器可作为集成光学回路的光源 (已实现边长10-30微米的激光器激射)。

- 利用TM模可研制出半径低达1微米的微腔激光器，而且纵向只要普通的半导体波导结构，不须强折射率波导，有希望研制出结构简单的电注入单光子源。